Title: UBAP2L-dependent coupling of PLK1 localization and stability during mitosis

Authors: Lucile Guerber[1, 2, 3, 4, #], Evanthia Pangou[1, 2, 3, 4, #,*], Aurore Vuidel[1, 2, 3, 4, 5], Yongrong Liao[1, 2, 3, 4], Charlotte Kleiss[1, 2, 3, 4], Erwan Grandgirard[1, 2, 3, 4] and Izabela Sumara[1, 2, 3, 4,*]

Affiliations:

[1] Institut de Génétique et de Biologie Moléculaire et Cellulaire (IGBMC), Illkirch, France.
[2] Centre National de la Recherche Scientifique UMR 7104, Strasbourg, France.
[3] Institut National de la Santé et de la Recherche Médicale U964, Strasbourg, France.
[4] Université de Strasbourg, Strasbourg, France.
[5] Current address, Ksilink, Strasbourg, France

[#] **These co-first authors contributed equally to this work**

***Correspondence:** Izabela Sumara Email: sumara@igbmc.fr and Evanthia Pangou Email: pangoue@igbmc.fr, Institute of Genetics and Molecular and Cellular Biology (IGBMC), Illkirch, France, Phone: +33 3 88 65 35 21, Fax: +33 3 88653201

Abstract

PLK1 is a key regulator of mitosis whose protein levels and activity fluctuate during cell cycle. PLK1 dynamically localizes to distinct mitotic structures to regulate proper chromosome segregation. However, the molecular mechanisms linking localized PLK1 activity to its protein stability remain elusive. Here, we identify the Ubiquitin-Binding Protein 2-Like (UBAP2L) protein that regulates both dynamic removal of PLK1 from kinetochores and PLK1 protein stability during mitosis. We demonstrate that UBAP2L localizes to kinetochores in a PLK1-dependent manner and that UBAP2L depletion leads to the abnormal retention of PLK1 at kinetochores and segregation defects. We show that C-terminal domain of UBAP2L mediates its function on PLK1 and that UBAP2L specifically regulates PLK1 and no other mitotic factors. We demonstrate that inhibited kinetochore removal of PLK1 in UBAP2L-depleted cells, increases PLK1 stability after mitosis completion and results in aberrant PLK1 kinase activity in interphase and cellular death. Overall, our data suggest that UBAP2L is required to fine-tune PLK1 signaling in human cells.

Graphical Abstract

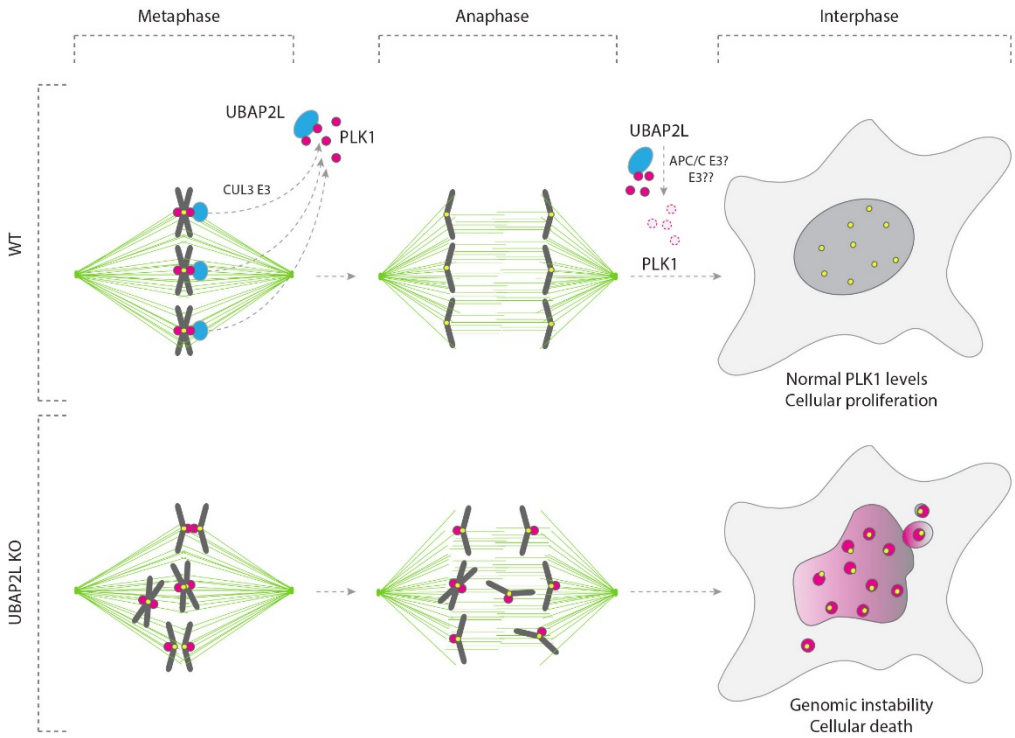

Introduction

Protein kinases represent key regulatory elements of the mitotic cycle, transferring phosphorylation signals to critical effectors (Nigg, 2001). Polo-like kinase 1 (PLK1) represents one of the key mitotic enzymes ensuring both mitotic entry as well as fidelity of genome segregation, mitotic exit and cytokinesis (Schmucker and Sumara, 2014; Combes et al., 2017; Petronczki et al., 2008) and remains an attractive target for anticancer therapies (Chiappa et al., 2022; Strebhardt, 2010). PLK1 is a serine/threonine kinase with an enzymatic domain at its N-terminal and a Polo-Box domain (PBD) at its C-terminal part, the latter representing a unique feature of the PLK kinase family and conferring specificity to phosphorylation substrates (Strebhardt, 2010; Barr et al., 2004; Zitouni et al., 2014). Its expression is cell cycle dependent, with PLK1 levels peaking at G2/M transition and dropping during mitotic exit and in early G1 (Golsteyn et al., 1995; Bruinsma et al., 2012) owing to the proteasomal degradation of PLK1 mediated through proteolytic ubiquitylation by the anaphase promoting complex/cyclosome (APC/C) E3 ubiquitin ligase (Lindon and Pines, 2004).

During mitosis PLK1 undergoes several post-translational modifications which fine-tune its dynamic localization, stability and activation/inactivation at several structures including the centrosomes, the kinetochores, the central spindle and the midbody (Schmucker and Sumara,

2014). PLK1 is enriched at kinetochores from prometaphase till metaphase stages through the interaction of its PBD with phosphorylated kinetochore receptors including budding uninhibited by benzimidazole 1 homolog (BUB1), BUBR1, and inner centromere protein (INCENP) (Elowe et al., 2007; Goto et al., 2006; Qi et al., 2006). At kinetochores, PLK1 regulates stability of kinetochore-microtubule (KT-MT) attachments and correct chromosome alignment (Elowe et al., 2007). Consequently, downregulation of PLK1 levels or inhibition of its kinase activity leads to spindle assembly checkpoint (SAC) potentiation and mitotic death (Sumara et al., 2004; Lenart et al., 2007). Interestingly, most of the PLK1 protein is removed from kinetochores during metaphase upon establishment of stable KT-MT attachments to allow for SAC silencing and anaphase onset (Elowe et al., 2007; Maia et al., 2012; Liu et al., 2012). Our previous studies have shown that PLK1 is a substrate for non-proteolytic CUL3-mediated ubiquitylation (Beck et al., 2013) prior to anaphase. CUL3 in complex with the substrate specific adaptor protein KLHL22 mono-ubiquitylates PLK1 within its PBD domain and interferes with phospho-receptors' binding, leading to the timely removal of PLK1 from kinetochores and faithful genome segregation. This modification is counteracted by the opposing function of the deubiquitylase (DUB) USP16 (Zhuo et al., 2015) that promotes proper chromosome alignment in early mitosis. Thus, both dynamic localization and protein stability of PLK1 are tightly regulated by phosphorylation- and ubiquitylation-based signals to ensure proper mitotic progression and genome stability. However, the exact molecular mechanisms linking the regulation of localized activity of PLK1 to its protein stability remain elusive.

Ubiquitin-Binding Protein 2-Like (UBAP2L, also known as NICE-4) is a highly conserved ubiquitin- and RNA-binding protein with versatile roles in multiple signaling cascades and cellular functions (Guerber et al., 2022). While UBAP2L has been mostly studied in the context of stress response signaling (Cirillo et al., 2020; Huang et al., 2020), recent evidence suggests that it can be involved in regulating mitotic progression (Maeda et al., 2016). UBAP2L is methylated within its RGG domain located at the N-terminal part and this modification was shown to promote the stability of KT-MT attachments, ensuring accurate chromosome distribution (Maeda et al., 2016). However, it remains unknown whether additional mechanisms to the reported methylation can actively drive the role of UBAP2L in cell division and what is the identity of direct downstream targets of UBAP2L during mitosis. In this study we provide evidence that UBAP2L can regulate both the dynamic localization of PLK1 and its protein stability in an RGG-domain independent manner. We demonstrate that UBAP2L localizes to kinetochores in a PLK1-dependent manner during mitosis and regulates timely dissociation of PLK1 from these structures and proper mitotic progression. Cells depleted for UBAP2L are characterized by mitotic delay, aberrant chromosome segregation, micronuclei and nuclear atypia. UBAP2L depletion impairs the removal of PLK1 from kinetochores prior to anaphase, increases its stability after mitosis completion and results in elevated PLK1 kinase activity in interphasic cells. Importantly, several defective mitotic phenotypes in UBAP2L depleted cells can be fully restored upon PLK1 inhibition, suggesting that the genomic instability observed upon UBAP2L depletion can be directly coupled to aberrant PLK1 mitotic signaling.

Results

UBAP2L regulates proper chromosome segregation during mitosis.

To identify novel ubiquitin-related factors with a potential role in mitosis, we previously performed a high-content visual siRNA screen in HeLa cells for known and predicted human ubiquitin-binding domain (UBD) proteins (Krupina et al., 2016) and we assessed phenotypes of irregular nuclear shape which is often the result of chromosome segregation defects (Jevtić et al., 2014). UBAP2L was among the top hits of the screen (Krupina et al., 2016), as its depletion led to increased number of cells displaying polylobed nuclei and multinucleation, phenotypes highly comparable to those observed upon down-regulation of the positive control CUL3 (Fig. S1A) (Maerki et al., 2009; Sumara et al., 2007). Interestingly, UBAP2L has been proposed to be involved in mitotic progression via its methylation by the arginine methyltransferase PRMT1 which is required for the formation of KT-MT attachments and chromosome alignment (Maeda et al., 2016) but the direct downstream targets of UBAP2L important for mitotic progression are currently unknown.

In order to corroborate our screening results and to further dissect the precise role of UBAP2L during mitosis, we deleted UBAP2L in HeLa cells using CRISPR/Cas9-mediated gene editing (Fig. S1B and S1C) and performed time-lapse live video microscopy (Fig. 1A and Videos S1-4). UBAP2L Knock-Out (KO) cell line displayed significant delay in mitotic entry and in timing from prophase to anaphase relative to isogenic wild-type (WT) control cell line (Fig. 1A-C). Moreover, UBAP2L KO cells were characterized by chromosome alignment defects and DNA bridges during anaphase and telophase, after which cells either exited mitosis as polyploid cells in the presence of accumulated micronuclei or died after prolonged mitotic arrest (Fig. 1A, and 1D-G). The presence of micronuclei and nuclear atypia in UBAP2L depleted cells was further confirmed in additional cell lines derived from colorectal cancer (DLD-1) (Fig. S1D-E) and osteosarcoma (U2OS) (Fig. S1F-G), respectively. Importantly, the mitotic defects observed in UBAP2L KO cells did not seem to be the consequence of pre-existing genomic instability, since UBAP2L KO cells that entered mitosis with both normal (Fig. 1A, second row and Video S2) and abnormal (Fig. 1A, third row and Video S3) nuclear shape, displayed equally severe segregation errors. Our results suggest that UBAP2L regulates proper and timely chromosome segregation during mitosis.

UBAP2L regulates PLK1 levels and activity.

Considering the fact that UBAP2L has been proposed to interact with CUL3 complexes (Bennett et al., 2010), we next aimed to understand if components of the CUL3 mitotic signaling (Jerabkova and Sumara, 2019) are linked to UBAP2L and its function during mitotic progression. While UBAP2L depletion did not affect the expression and localization of Aurora A (AURA) and Aurora B (AURB) in mitotically arrested cells, it increased the levels of PLK1 (Fig. S2A). UBAP2L depletion did also not affect the localization of other mitotic factors such as Cyclin B1 (Fig. S2A), suggesting that deletion of UBAP2L affects specifically PLK1 and not as an indirect effect of

perturbed cell cycle progression. Western Blot analysis of cells synchronized in G1/S phase, revealed that although UBAP2L downregulation by specific siRNA (Cirillo et al., 2020) had no effect on the protein levels of Cyclin B1, AURA and AURB, it resulted in increased levels of PLK1 relative to control-depleted cells (Fig. 2A), confirming dysregulation of PLK1 signaling in the absence of UBAP2L. Consistently, immunofluorescence analysis showed that UBAP2L downregulation led to an increased number of cells with enriched nuclear localization of PLK1 (Fig. 2B-D). These results were confirmed in UBAP2L KO cells which displayed increased PLK1 protein levels and nuclear localization during interphase (Fig. 2E-H), without affecting Cyclin B1, AURA and AURB expression (Fig. 2E and Fig. S2B-E). Subcellular fractionation assays further confirmed nuclear accumulation of PLK1 during interphase in UBAP2L KO cells relative to WT cells (Fig. 2I). The effect of UBAP2L on PLK1, prompted us to test whether UBAP2L might also regulate additional PLK family members but no detectable changes were observed upon UBAP2L downregulation in the total protein levels of PLK2, PLK3 and PLK4 (Fig. 2J). Interestingly, PLK1 activatory phosphorylation on Thr210 as well as the PLK1 phospho-substrate BubR1 (Elowe et al., 2007) were increased in the absence of UBAP2L (Fig. 2J) in interphasic cells upon UBAP2L depletion. Overall, our results suggest that UBAP2L regulates PLK1 protein levels and activity without affecting other major mitotic factors.

The increased PLK1 levels observed in UBAP2L KO cells could be either due to enhanced protein translation or reduced protein degradation. To distinguish between the two possibilities, we analyzed PLK1 protein levels in a time course of WT and UBAP2L KO cells treated either with the translation inhibitor cycloheximide (CHX), or with the proteasomal inhibitor MG132. In contrast to AURB, PLK1 protein levels remained stable up to 8h of CHX treatment in the absence of UBAP2L, while AURB and PLK1 were gradually degraded in WT cells, both during interphase (Fig. S3A) and in cells arrested in mitosis using the microtubule stabilizing agent paclitaxel (Fig. S3B). MG132 treatment increased the levels of total ubiquitin as expected but no additive effect was observed in PLK1 levels in UBAP2L depleted cells relative to WT cells (Fig. S3C). Taken together, our results suggest that UBAP2L may promote degradation of PLK1 and its function on PLK1 might be uncoupled from the regulation of cell cycle progression.

The C-terminal domain of UBAP2L mediates its function on PLK1.

Next, we aimed to understand if effects of UBAP2L on PLK1 levels and localization are specific to downregulation of UBAP2L and which functional domain of UBAP2L mediates its function on PLK1. Rescue experiments in UBAP2L KO cells ectopically expressing flag-tagged UBAP2L full length (FL) and/or UBAP2L protein fragments (Fig. 3A and 3B), revealed that nuclear accumulation of PLK1 in interphase could be efficiently restored by re-expression of UBAP2L FL or the UBAP2L C-terminal fragment but not the N-terminal fragment of UBAP2L (Fig. 3C and 3D). These findings argue that the function of UBAP2L on PLK1 is mediated through its C-terminal part and it might be disconnected from the reported role of the RGG domain on mitosis (Maeda et al., 2016), which may regulate other, yet to be identified mitotic factors.

The Domain of Unknown Function (DUF) located within the C-terminal part of UBAP2L is responsible for its interaction with core components of stress granules (SGs) such as the Ras GTPase-activating protein-binding protein (G3BPs), thus enabling their correct assembly upon stress signaling (Huang et al., 2020). In order to exclude the possibility that UBAP2L-mediated regulation of PLK1 is linked to stress signaling, we performed similar rescue experiments in the presence and absence of G3BP1 and G3BP2 (Fig. 4A, and 4D). Importantly, G3BPs depletion by specific siRNAs (Cirillo et al., 2020) (Fig. 4D) did not abolish the rescue potential of UBAP2L FL and C-terminal part on PLK1 nuclear accumulation (Fig. 4A-C), suggesting that UBAP2L-mediated regulation of PLK1 can be uncoupled from the previously established function of the UBAP2L C-terminal domain in G3BP1/G3BP2-dependent SGs assembly.

Since absence of UBAP2L led to segregation errors frequently followed by cellular death (Fig. 1A fourth row, G and Video S4), we tested whether UBAP2L might also regulate cell proliferation. In accordance with studies showing that cells harboring accumulated errors during cell division often display reduced survival (Cheng and Crasta, 2017), UBAP2L KO cells displayed significantly reduced long-term proliferation capacity and viability (Fig. 3E-G). Re-expression of UBAP2L FL or the UBAP2L C-terminal fragment but not the UBAP2L N-terminal protein part fully rescued cell survival and partially rescued cell proliferation (Fig. 3E-G). These results further strengthen our hypothesis that UBAP2L emerges as an important factor for fine-tuning PLK1 levels and localization and ultimately cellular proliferation and survival.

UBAP2L does not regulate PLK1 levels and localization in G2 cell cycle stage.

Since we observed increased protein levels of PLK1 in interphasic cells (Fig. 2) likely due inhibition of protein degradation (Fig. S3A and S3B) in the absence of UBAP2L, we next aimed to understand during which cell cycle stage UBAP2L controls PLK1 stability. Indeed, PLK1 protein levels strongly fluctuate during cell cycle progression, increasing in G2 phase, peaking during mitosis and decreasing again during mitotic exit and in early G1 (Golsteyn et al., 1995; Bruinsma et al., 2012). For this purpose, we analyzed PLK1 levels and localization by synchronizing cells in different cell cycle stages using several treatments: double thymidine block for G1/S transition, hydroxyurea for the S phase and CDK1 inhibitor RO3306 for G2 (Fig. 5A), as previously described (Agote-Arán et al., 2021). Western blotting with antibodies to several cell cycle markers confirmed efficient synchronization of cells where Cyclin E was accumulated during G1/S transition and decreased along the S phase, Cyclin A levels gradually increased peaking in the S phase, and Cyclin B1 gradually increased reaching the highest concentration in G2 (Fig. 5B). Interestingly, the number of cells expressing PLK1, as well as PLK1 nuclear accumulation, were increased in UBAP2L KO cells during G1 and S phases, but no changes were detected during G2 stage relative to WT cells (Fig. 5A, 5C and 5D). These results suggest that UBAP2L rather seems to regulate PLK1 levels during or after mitotic exit and not prior to mitotic entry.

The finding that PLK1 accumulates in the nucleus in a dotty pattern in G1/S when UBAP2L is depleted, triggered us to investigate in more detail how UBAP2L regulates the spatiotemporal

dynamics of PLK1. Is PLK1 nuclear enrichment enhanced specifically during G1 or is it a consequence of its aberrant expression and localization during mitosis? To test the possibility that UBAP2L might regulate the recruitment of PLK1 at the kinetochores during G1 which is known to occur in order to promote faithful CENP-A deposition at the centromeres in a Mis18 complex-dependent manner (McKinley and Cheeseman, 2014), we depleted Mis18α and CENP-A in G1 synchronized WT and UBAP2L KO cells (Fig. S4A) and quantified the percentage of cells displaying PLK1 kinetochore enrichment. Interestingly, neither Mis18α nor CENP-A depletion could rescue the PLK1 kinetochore accumulation observed in UBAP2L KO cells (Fig. S4A-E), thereby suggesting that UBAP2L depletion does not seem to trigger the premature kinetochore recruitment of PLK1 during G1 but might rather regulate its removal prior to anaphase and mitotic exit.

UBAP2L localizes to kinetochores during mitosis.

First, we tested if UBAP2L may directly regulate kinetochore dynamics of PLK1 by localizing to these structures during mitosis. Immunofluorescence microscopy analysis of endogenous UBAP2L revealed that this protein despite being mostly cytoplasmic, can also weakly localize to kinetochores in cells arrested in prometaphase using the Eg5 inhibitor STLC (Fig. 6A). Intriguingly, decrease of PLK1 activity using the specific kinase inhibitor BI2536 (Lenart et al., 2007), led to increased recruitment of UBAP2L to kinetochores (Fig. 6A and 6B), despite the total levels of UBAP2L being reduced upon BI2536 treatment (Fig. 6C). The kinetochore enrichment of UBAP2L in prometaphase arrested cells was more pronounced upon PLK1 down-regulation, with endogenous UBAP2L accumulating in cytoplasmic and/or chromosomal aggregates which often but not always co-localized with individual pairs of sister kinetochores (Fig. 6D and 6E), while the total levels of UBAP2L were reduced in PLK1-downregulated cells (Fig. 6F). These results suggest that the kinetochore localization pattern of UBAPL2 might be dynamic and dependent on presence and localized activity of PLK1 and possibly on microtubule attachment status.

To further test the hypothesis that the association of UBAP2L to kinetochores is PLK1- and attachment-dependent, we synchronized cells in several mitotic stages using the Eg5 inhibitor Monastrol block and release protocol as described previously (Pangou et al., 2021) and analyzed the localization of endogenous UBAP2L. We observed increased recruitment of UBAP2L to kinetochores during metaphase relative to prometaphase stages (Fig. 7A and 7B), which correlates with reported decrease in localized PLK1 activity upon attachment stabilization and represents the mitotic stage when PLK1 undergoes removal from kinetochores. Our findings on the kinetochore-associated fraction of endogenous UBAP2L were also confirmed by analyzing the mitotic localization of ectopically expressed flag-tagged UBAP2L FL and UBAP2L protein fragments. Interestingly, both UBAP2L FL and the UBAP2L C-terminal fragment mimicked the phenotype observed for the endogenous UBAP2L upon PLK1 depletion, forming aggregates on chromosomes, a fraction of which accumulated on individual kinetochores, while the N-terminal fragment of UBAP2L was not detected at the kinetochores and rather displayed a diffused

localization pattern in the cytoplasm (Fig. 7C). Overall, these results are in line with the fact that UBAP2L mediates its function on PLK1 via its C-terminal domain (Fig. 3) specifically at kinetochores.

UBAP2L removes PLK1 from kinetochores.

Having demonstrated that UBAP2L does not interfere with the kinetochore recruitment of PLK1 during G1 and that UBAP2L localizes to kinetochores preferentially during metaphase, we then wondered whether UBAP2L is involved in dissociating PLK1 from kinetochores prior to anaphase onset. To this end, we assessed the effect of UBAP2L depletion on PLK1 localization in mitotically synchronized cells treated with Monastrol and collected at different time points after the release. Immunofluorescence analysis revealed that as early as in prometaphase, PLK1 displayed increased levels as well as cytoplasmic aggregates upon UBAP2L depletion relative to control cells (Fig. 8A). Moreover, during telophase and cytokinesis stages (1h and 30 min post release), UBAP2L depletion not only led to enrichment of PLK1 signals at the midbody, but also PLK1 was aberrantly retained at the kinetochores relative to control cells (Fig. 8A-C). Finally, when UBAP2L depleted cells exited mitosis and entered into the subsequent interphase (3h, 4 h and 30min post release), PLK1 was still highly enriched at the kinetochores compared to control cells in which PLK1 was no longer detected at these structures (Fig. 8A and 8C). These results suggest that UBAPL2 is required for the efficient removal of PLK1 from the kinetochores during mitosis. Interestingly and consistent with previous results on PLK1 stability in G1 cells, UBAP2L downregulation led to reduced PLK1 degradation after release from Monastrol (Fig. 8D). To further corroborate these findings, we generated a HeLa PLK1-eGFP knock in (KI) cell line, which displayed no aberrant phenotypes in terms of PLK1 expression, localization and mitotic progression relative to isogenic PLK1-WT control cell line (Fig. S5A-E). Live video imaging in the PLK-eGFP KI cells synchronized with double thymidine block and release, further confirmed the enhanced expression of PLK1 from prophase to cytokinesis at the kinetochores, spindle poles, midzone and midbody, as well as its aberrant accumulation on kinetochores from anaphase to cytokinesis in the absence of UBAP2L (Fig. 8E and Videos S5, S6). Altogether, our results indicate that UBAP2L emerges as an important factor for the efficient and timely removal of PLK1 from the kinetochores during metaphase to anaphase transition and for the regulation of PLK1 protein stability.

UBAP2L may regulate interaction of PLK1 with CUL3 to ensure faithful chromosome segregation.

Timely kinetochore removal of PLK1 during metaphase and chromosome segregation is regulated by CUL3-mediated mono-ubiquitylation of PLK1 (Beck et al., 2013). Although this modification does not affect the protein stability of PLK1 (Beck et al., 2013), we reasoned that possible involvement of UBAP2L in CUL3 pathway could explain, at least partially, the observed localization defects of PLK1 in UBAP2L-depleted cells. Indeed, a proteomics study has suggested that UBAP2L interacts with CUL3 complexes in human cells (Bennett et al., 2010)

Co-immunoprecipitation (co-IP) assays in mitotically synchronized cells showed that endogenous UBAP2L could efficiently interact with CUL3 and its substrate specific adaptor KLHL22 as well as with PLK1, relative to IgG control, but not with AURB which is another known mitotic ubiquitylation substrate of CUL3 (Beck et al., 2013; Courtheoux et al., 2016; Krupina et al., 2016; Maerki et al., 2009; Moghe et al., 2012; Sumara et al., 2007) (Fig. 9A). To test the hypothesis that CUL3-mediated regulation of PLK1 during mitosis could be, at least to some extent, dependent on UBAP2L, endogenous co-IP of PLK1 was performed in the presence or absence of UBAP2L. UBAP2L depletion reduced the PLK1 interaction with CUL3 relative to control cells expressing UBAP2L (Fig. 9B), indicating that UBAP2L may be an essential component of this pathway.

Since UBAP2L, but not CUL3 (Beck et al., 2013), can also regulate stability of PLK1, we next aimed at understanding if polyubiquitylation status of PLK1 can be regulated by UBAP2L. To this end, we performed co-IP of GFP-PLK1 in the presence of proteasomal inhibitor MG132 under denaturing conditions in UBAP2L KO and in WT cells. Interestingly, we observed a significantly less pronounced polyubiquitin modification on immunoprecipitated GFP-PLK1 in cells depleted for UBAP2L (Fig. 9C). These results suggest that UBAP2L may control both timely non-proteolytic removal of PLK1 from kinetochores with help of CUL3 E3-ligase as well as ubiquitin-mediated proteolysis of PLK1 during mitotic exit. The identity and precise mechanism of the possible additional E3-ligase involved in UBAP2L regulation of PLK1 stability remains to be determined in future.

To prove that the chromosome segregation and other mitotic errors observed in cells lacking UBAP2L could be directly linked to increased levels and activation of PLK1 we performed rescue experiments using the chemical inhibitor BI2536 of PLK1 kinase (Lenart et al., 2007). To this end, we inhibited PLK1 activity after release from Monastrol treatment at different time points and we compared the rate of segregation errors in UBAP2L-downregulated cells relative to control cells. BI2536 efficiently restored PLK1 activity to basal levels in UBAP2L depleted cells as verified by its auto-phosphorylation on Thr210 (Fig. 9D). Interestingly, BI2536 treatment fully rescued all types of erroneous mitotic phenotypes observed in UBAP2L depleted cells, including chromosome misalignment in metaphase, DNA bridges in anaphase and telophase and micronuclei formation after cytokinesis completion (Fig. 9E-H). Our results suggest that aberrant PLK1 activity resulting from increased stability of this kinase is the leading cause for mitotic defects observed in UBAP2L-depleted cells.

Discussion

In summary, our study provides novel insights into how PLK1 by UBAP2L is spatiotemporally regulated during mitotic progression. We propose that UBAP2L associates with kinetochore structures during metaphase in order to efficiently promote both the kinetochore removal and the degradation of PLK1 prior to anaphase as a means to ensure faithful chromosome segregation. We demonstrate that UBAP2L depleted cells are characterized by significant mitotic delay, severe segregation errors and micronuclei formation, phenotypes that can be directly linked to aberrant PLK1 kinase activity. We provide evidence that in the absence of UBAP2L-mediated signaling,

PLK1 is abnormally retained at the kinetochore and fails to get degraded during mitotic exit, resulting in excessive PLK1 expression and kinase activity in the subsequent interphase, which may ultimately cause genomic instability and cell death.

How does UBAP2L regulate mitosis?

Mitosis is a fundamental process in eukaryotes, where steps such as chromosome congression and chromosome alignment need to be precisely fine-tuned to ensure high fidelity of cell division (McIntosh, 2016). Phosphorylation and ubiquitylation pathways are tightly interconnected during mitosis, however how exactly these signaling cues are integrated and orchestrated in a space–time-dependent manner remains not fully understood. Here, we identify the ubiquitin-binding protein UBAP2L as a novel regulator of PLK1 controlling both its localization and protein stability. We show that UBAP2L regulates PLK1 in a cell-cycle specific manner, with UBAP2L depletion leading to enhanced protein levels and kinetochore enrichment of PLK1 in mitosis and in the subsequent G1/S, while we did not observe any effect during G2 (Fig. 5). UBAP2L interacts with PLK1 in mitotically synchronized cells (Fig. 9A), thereby licensing the kinetochore removal of PLK1 prior to anaphase (Fig. 8), while having no effect on the kinetochore recruitment of PLK1 during G1/S (Fig. S4). Importantly, we show that the regulatory effect of UBAP2L towards PLK1 is specific and can be uncoupled from cell cycle progression, since UBAP2L does not interact (Fig. 9A) and does not modulate the protein levels and/or localization of other mitotic factors including AurA, AurB, and Cyclin B1 (Fig. 2 and S2), nor other PLK family members (Fig. 2J).

This specific UBAP2L-PLK1 signaling could potentially be explained by the fact that a fraction of UBAP2L dynamically localizes at the kinetochore during prometaphase and metaphase (Fig. 7), indicating that UBAP2L exerts its mitosis-related functions specifically at these mitotic structures and stages. PLK1 is known to be enriched at kinetochores from prometaphase till metaphase (Elowe et al., 2007), while at these early mitotic stages AURB mostly localizes at the inner centromere (Yamagishi et al., 2010) and AURA, Cyclin B1, PLK2, PLK3 and PLK4 are mostly enriched at the mitotic spindle and the centrosomes (Fournier et al., 2016; Jiang et al., 2006; Pines, 1997; Sugimoto et al., 2002; Warnke et al., 2004). We could therefore speculate that the mitotic role of UBAP2L can be attributed to its kinetochore associated fraction which provides access to kinetochore substrates such as PLK1. Therefore, it would be worth investigating whether additional kinetochore proteins might be under UBAP2L regulation to ensure mitotic fidelity.

Of interest, UBAP2L has also been proposed to be phosphorylated during mitosis (Dephoure et al., 2008; Maeda et al., 2016), but the kinase involved or the underlying mechanisms are currently unknown. Our results demonstrate that the kinetochore associated fraction of UBAP2L is dependent on PLK1 activity/expression (Fig. 6). Given that the C-terminal domain of UBAP2L is predicted to harbor several PLK1 consensus motifs (Santamaria et al., 2011), it would be interesting to address the possibility of UBAP2L being a direct phosphorylation target of PLK1 or an indirect substrate via CDK1 priming phosphorylation (Parrilla et al., 2016). Such a regulatory feedback loop has already been described for PLK1/USP16 (Zhuo et al., 2015, 16) and would

advance our understanding on how PLK1 can dynamically drive its own localized activity to ensure fidelity of cell division.

Role of UBAP2L C-terminal domain in the regulation of PLK1

Our data demonstrate that the uncontrolled kinetochore PLK1 retainment and the elevated PLK1 protein stability during mitotic exit observed in UBAP2L depleted cells are mediated specifically and exclusively through UBAP2L. The phenotypes described for segregation errors, polyploidy, specific effect on PLK1 and not on other mitotic factors are corroborated by specific siRNAs against UBAP2L (Cirillo et al., 2020) and by CRISPR-mediated genetic depletion of UBAP2L, excluding the possibility of an off-target or a compensatory effect. Our rescue experiments provide evidence that both PLK1 aberrant kinetochore accumulation (Fig. 3C) and cell survival (Fig. 3E) can be entirely rescued by overexpression of the C-terminal domain of UBAP2L, but are not dependent on its N-terminal domain that was until now considered to mediate the mitotic role of UBAP2L (Maeda et al., 2016). Moreover, we show that the accumulated micronuclei observed in UBAP2L depleted cells during mitotic exit is directly linked to aberrant PLK1 expression/activity in these cells (Fig. 9E). However and in line with our results, the study by Maeda and colleagues reported that an extra sequence after the UBA-RGG domain is essential for proper mitotic progression, while overexpression of the UBA-RGG domain alone cannot restore the multinuclear phenotype observed in UBAP2L-depleted cells (Maeda et al., 2016). Altogether, these results argue for the existence of at least two distinct pathways responsible for mediating the role of UBAP2L during mitosis. One dependent on PRMT1 methylation with yet unknown UBAP2L downstream mitotic targets (Maeda et al., 2016) and one dependent on UBAP2L kinetochore localization and on PLK1 activity as proposed in this study.

UBAP2L and in particular its C-terminus domain have been mostly studied in the context of SGs signaling (Cirillo et al., 2020; Huang et al., 2020; Youn et al., 2018). Our results show that depletion of core SGs components had no effect on the ability of UBAP2L FL and/or UBAP2L C-terminal fragment to fully restore the aberrant kinetochore accumulation of PLK1 (Fig. 4B-C), thus suggesting that the C-terminus domain of UBAP2L has an unexpected new role during mitosis that seems unrelated to its established role of G3BP1/G3BP2-dependent SGs signaling. Furthermore, the PRMT1-dependent UBAP2L methylation that is linked to accurate chromosome segregation, was recently reported to impair SG assembly (Huang et al., 2020), again indicating that the role of UBAP2L in mitosis and its effect on PLK1 does not interfere with its role is SGs signaling. Interestingly, SGs cannot be formed during mitosis and membraneless organelles (apart from centrosomes) are dissolved at G2/M transition in a kinase-dependent manner (Rai et al., 2018). It would be intriguing to speculate that UBAP2L may be subjected to phosphorylation during mitotic entry as a means to promote the dissolution of SGs, thereby shifting the interactions and functions of UBAP2L towards components of the mitotic machinery.

UBAP2L regulates both PLK1 localization and stability

How exactly does UBAP2L regulate PLK1 to ensure fidelity of cell division? Our data demonstrate that in cells lacking UBAP2L, not only PLK1 is abruptly retained at the kinetochore throughout mitosis (Fig. 8), but is also protected from degradation (Fig. S3), resulting in persistent PLK1 protein stability and activity in the interphasic cells. More specifically, we show that in the absence of UBAP2L, PLK1 is resistant to CHX treatment both in interphasic (Fig. S3A) and mitotic cells (Fig. S3B) and that the number of cells expressing PLK1 during interphase is significantly increased compared to control WT cells where PLK1 is only detected at basal levels (Fig. 2). Furthermore, we show that UBAP2L depletion does not interfere with the kinetochore recruitment of PLK1 in early G1/S (Fig. S4), but it impairs PLK1 kinetochore removal during mitosis (Fig. 8). Finally, we observe that loss of UBAP2L weakens the mitotic interaction between PLK1 and CUL3 (Fig. 9B) and results in markedly decreased polyubiquitin modification of PLK1 under denaturing conditions (Fig. 9C).

Cullin-RING ubiquitin ligases (CRLs) are the largest family of E3 ubiquitin ligases that regulate both proteolytic and non-proteolytic ubiquitin signals in a large variety of cellular processes (Jang et al., 2020; Jerabkova and Sumara, 2019). Accumulating evidence suggests that CUL3 emerges as a critical regulator of cell division by regulating critical mitotic kinases such as PLK1, AURA and AURB (Beck et al., 2013; Krupina et al., 2016; Maerki et al., 2009; Sumara et al., 2007; Courtheoux et al., 2016; Moghe et al., 2012). However, we still lack sufficient knowledge regarding the molecular identity and function of additional factors that act in concert with CUL3 to precisely define the cellular fate of mitotic substrates and subsequently cell cycle progression. It was recently proposed that both CRL substrate recruitment as well as CRL complex assembly are dependent on the coordinated actions of specific co-adaptors and inhibitors to ensure their function in time and space (Akopian et al., 2022). Here, we demonstrate that UBAP2L specifically regulates the protein levels and localization of PLK1 but of no other mitotic targets of CUL3 including AURA and AURB (Fig. 2 and S2). Moreover, UBAP2L directly interacts with PLK1, CUL3 and KLHL22, but not with AURB during mitosis (Fig. 9A). Given the loss of interaction between CUL3 and PLK1 observed upon UBAP2L depletion (Fig. 9B), our data indicate that UBAP2L might be important for the recognition of PLK1 by the KLHL22/CUL3 complex. This could, at least to some extent, explain the phenotype of PLK1 being unable to get efficiently removed from kinetochores in the absence of UBAP2L and could suggest that UBAP2L might act as a co-adaptor for CUL3 to ensure its access to PLK1 at the kinetochore prior to anaphase. Further studies are needed to explore whether UBAP2L might decipher the versatility of the CUL3-based ubiquitin code during cell division.

Intriguingly, the additional regulation of PLK1 by UBAP2L at the level of protein stability, suggests that UBAP2L might also regulate PLK1 independently of the CUL3-based pathway via yet uncharacterized mechanisms. PLK1 is ubiquitylated by the APC/C E3 ubiquitin ligase in anaphase via its interaction with FZR1/CDH1, which provides the signal for the proteasomal-dependent degradation of PLK1 during mitotic exit (Lindon and Pines, 2004). One possibility would be that in the absence of UBAP2L the affinity of PLK1 towards CDH1 is reduced or shifted towards CDC20, therefore leading to increased PLK1 protein stability during mitotic exit. Still,

we cannot exclude that the UBAP2L-driven proteolytic signals on PLK1 might involve other E3 ligases independent of the APC/C established mechanism, or that CUL3 might associate with unknown adaptors/inhibitors (Akopian et al., 2022) which in turn activate proteolytic ubiquitylation on PLK1. To our knowledge, such a dual regulation for PLK1 in terms of both stability and localization has only been described in one more study which addressed the role of NUMB in mitosis, a protein mostly known for its function in progenitor cell fate determination (Gulino et al., 2010). The authors show that NUMB depletion resulted in reduced PLK1 protein stability and in aberrant centrosomal localization of PLK1 at both metaphase and anaphase, leading to disorganized γ-tubulin recruitment to centrosomes (Schmit et al., 2012). Our work is the first to report a unique role for UBAP2L in converging both proteolytic and non-proteolytic ubiquitin signals on PLK1 in order to ensure fidelity of mitotic progression. How exactly those two UBAP2L-dependent signaling cascades communicate with each other to precisely regulate PLK1 in time and space remains to be addressed in future studies.

Possible consequences of aberrant PLK1 signaling

Mitotic perturbations are causally linked to aneuploidy and genomic instability (S. Pedersen et al., 2016). Phosphorylation and ubiquitylation pathways are tightly interconnected in mitosis and it is important to understand these links in the context of carcinogenesis. PLK1 is misregulated in human cancers and small molecule inhibitors targeting PLK1 are currently being explored for cancer treatment (Chiappa et al., 2022). However, preclinical success with currently available PLK1 inhibitors has not translated well into clinical success, highlighting the need for a complete understanding of upstream PLK1 regulatory mechanisms. In our view, combined therapies targeting other relevant pathways together with PLK1 may be vital to combat issues observed with monotherapy, especially resistance. In addition, research should also be directed towards understanding the mechanisms regulating localized activity of PLK1 and designing additional next generations of specific, potent PLK1 inhibitors to target cancer (Gutteridge et al., 2016). Of interest, the signaling pathways mediating the recruitment and the removal of PLK1 at and from kinetochore structures are characterized by several layers of regulation and complexity, raising the possibility that distinct pools of PLK1 may exist at kinetochores (Lera et al., 2016).

We provide evidence that UBAP2L depletion inhibits the kinetochore removal of PLK1 and increases its stability after mitosis completion, resulting in aberrant PLK1 kinase activity in interphasic cells, which may ultimately cause genomic instability and cellular death. What could be the potential consequences for cells entering the subsequent cell cycle in the presence of high PLK1 activity? PLK1 has a largely unexplored and unconventional functional territory beyond mitosis especially in processes such as DNA replication, transcription and damage checkpoint recovery (Kumar et al., 2017). Our study suggests that the accumulated micronuclei observed in UBAP2L depleted cells during mitotic exit is directly linked to aberrant PLK1 expression/activity in these cells (Fig. 9E and 9H). Micronuclei display highly heterogeneous features regarding the recruitment or retainment of replication, transcription and DNA damage response factors, ultimately being associated with chromosomal instability (Krupina et al., 2021). Interestingly,

PLK1 has been shown to regulate RNAPIII-dependent transcription, switching from activation to repression based on its activatory status (Fairley et al., 2012), while a recent study implicated UBAP2L in the ubiquitylation and degradation of RNAPII through the recruitment of a Cullin-based ubiquitin complex (Herlihy et al., 2022). We could therefore speculate that cells with defective UBAP2L-PLK1 signaling would be more prone to unbalanced transcription which would further hijack their genome fidelity, a concept worth to be investigated in the future.

Finally, growing evidence suggests that UBAP2L is overexpressed in a variety of cancers where it displays oncogenic properties by interfering with signaling pathways that promote cancer cell proliferation, tumor vascularization, migration, invasion and metastasis (Guerber et al., 2022). While the oncogenic potential of UBAP2L renders it an attractive candidate for therapy, the results presented in our study linking its depletion to aberrant PLK1 activation and perturbed cell division, rather indicate that targeting UBAP2L might be a strategy that should be applied with caution. The pathway described in our study could maybe direct research efforts towards the synergistic inhibition of UBAP2L and PLK1 in specific cancer types.

Figures Legends

Fig. 1. UBAP2L regulates proper chromosome segregation during mitosis.

(A) Spinning disk time-lapse microscopy of WT and UBAP2L KO HeLa cells synchronized with double thymidine block and release (DTBR) in mitosis. The selected frames of the movies are depicted and the corresponding time is indicated in minutes. SiR-DNA was used for DNA staining. Scale bar, 8µm.

(B and C) The time of mitotic entry **(B)** and from prophase to anaphase **(C)** was quantified. At least 50 cells per condition were analyzed for each experiment. Red bar represents the mean. **(D-G)** The percentages of cells with misaligned chromosomes **(D)**, DNA bridges **(E)**, micronuclei **(G)** and dead cells **(H)** were quantified. At least 50 cells per condition were analyzed. Graphs represent the mean of five replicates ± standard deviation (SD) (two sample two-tailed t-test or one-way ANOVA with Dunnett's correction *P<0,05, **P<0,01, ***P<0,001, ****P<0,0001, ns=non-significant).

Fig. 2. UBAP2L regulates PLK1 levels and activity.

(A) Western blot (WB) analysis of G1/S synchronized HeLa cells lysates using DTB treated with non-targeting (siNT) or UBAP2L siRNA. Proteins molecular weight (MW) is indicated in kilo Daltons (kDa). WB is representative of three independent replicates.

(B-D) Immunofluorescence (IF) representative pictures of G1/S synchronized HeLa cells treated with the indicated siRNAs and quantification of the percentage of cells expressing PLK1 **(C)** or PLK1 nuclear intensity **(D)**. Scale bar, 5µm. At least 250 cells were quantified per condition for each replicate. Graphs depicted in **(C)** represent the mean of three replicates ± SD (two sample two-tailed t-test). Each dot of graphs **(D)** represents PLK1 nuclear intensity in a single nucleus.

The measurements of three biological replicates are combined, red bars represent the mean (Mann-Whitney test). **P<0,01, ***P<0,001, ****P<0,0001).

(E) WB analysis of G1/S synchronized WT or UBAP2L KO HeLa cells lysates using DTB. Proteins MW is indicated in kDa. WB is representative of three independent replicates.

(F-H) IF representative pictures of G1/S synchronized WT or UBAP2L KO HeLa cells and quantification of the percentage of cells expressing PLK1 **(G)** or PLK1 nuclear intensity **(H)**. Scale bar, 5µm. At least 250 cells were quantified per condition for each replicate. Graphs depicted in **(G)** represent the mean of four replicates ± SD (one-way ANOVA with Dunnett's correction). Each dot of graphs **(H)** represents PLK1 nuclear intensity in a single nucleus. The measurements of four biological replicates are combined, red bars represent the mean (Mann-Whitney test). **P<0,01, ***P<0,001, ****P<0,0001).

(I) WT or UBAP2L KO G1/S synchronized HeLa cells were lysed and fractionated into cytoplasmic and nuclear fractions and analyzed by WB. Proteins MW is indicated in kDa.

(J) WB analysis of unsynchronized HeLa cells lysates treated with the indicated siRNAs. Proteins MW is indicated in kDa. WB is representative of three independent replicates.

Fig. 3. The C-terminal domain of UBAP2L mediates its function on PLK1.

(A) Schematic representation of UBAP2L protein fragments. Indicated numbers stand for aminoacids (aa).

(B) WB analysis of G1/S synchronized WT or UBAP2L KO HeLa cells lysates transiently transfected with the indicated flag-tagged UBAP2L protein fragments. Proteins MW is indicated in kDa. Arrows point to the migration of each fragment. WB is representative of three independent replicates.

(C, D) IF analysis of G1/S synchronized WT or UBAP2L KO HeLa cells transiently transfected with the indicated flag-tagged UBAP2L protein fragments and quantification of the percentage of cells expressing PLK1 **(D)**. Scale bar, 5µm. At least 100 cells per condition were quantified for each experiment. Graphs represent the mean of three replicates ± SD (one-way ANOVA with Sidak's correction *P<0,05, **P<0,01, ****P<0,0001, ns=non-significant).

(E-G) Colony formation assay of WT or UBAP2L KO HeLa cells transiently transfected with the indicated flag-tagged UBAP2L protein fragments and quantification of the individual colony area **(F)** and of the number of colonies **(G)** after 7 days of culture. Graphs represent the mean of three replicates ± SD (one-way ANOVA with Sidak's correction *P<0,05, **P<0,01, ****P<0,0001, ns=non-significant).

Figure 4. UBAP2L-mediated PLK1 regulation is G3BP1/2 independent.

(A-C) Representative IF images of WT or UBAP2L KO HeLa cells transiently transfected with the indicated flag-tagged UBAP2L constructs and control or G3BP1/2 siRNAs. Scale bar, 5µm. Quantification of the percentage of cells expressing PLK **(B)** and of PLK1 nuclear intensity **(C)** At least 150 cells were quantified per condition for each replicate. Graphs depicted in **(B)** represent the mean of three replicates ± SD (one-way ANOVA with Sidak's correction). Each dot of graphs

(C) represents PLK1 nuclear intensity in a single nucleus. The measurements of three biological replicates are combined, red bars represent the mean (Kruskal-Wallis test with Dunn's correction). *P<0,05, ***P<0,001, ****P<0,0001, ns=non-significant.
(D) WB analysis of the experiment described in (A). Proteins MW is indicated in kDa. WB is representative of three independent replicates.

Figure 5. UBAP2L does not regulate PLK1 levels and localization in G2 cell cycle stage.
(A) Representative IF pictures of WT or UBAP2L KO HeLa cells synchronized in G1/S using double thymidine block, in S using hydroxyurea or in G2 using CDK1 inhibitor RO 3306. Scale bar, 5µm.
(B) WB analysis of the experiment depicted in **(A)**. Proteins MW is indicated in kDa. WB is representative of three independent replicates.
(C-D) Quantification of PLK1 nuclear intensity **(C)** and of the percentage of cells expressing PLK1 **(D)**. At least 200 cells per condition were quantified for each replicate. Each dot of graphs **(C)** represents PLK1 nuclear intensity in a single nucleus. The measurements of three biological replicates are combined, black bars represent the mean. Graphs depicted in **(D)** represent the mean of three replicates ± SD (one-way ANOVA with Dunnett's correction or Mann-Whitney test *P<0,05, ****P<0,0001, ns=non-significant).

Figure 6. UBAP2L localizes to kinetochores during mitosis in a PLK1-dependent manner.
(A-B) Representative IF pictures of HeLa cells synchronized in mitosis using STLC and treated with DMSO or 50nM BI2536 **(A)** and quantification of the relative UBAP2L intensity at kinetochores (arbitrary units A.U.) **(B)**. ROIs are shown in the corresponding numbered panels. Scale bar, 5µm. At least 50 cells were quantified per condition for each experiment. Each dot represents UBAP2L/CREST intensity ratio at a single pair of kinetochores. The measurements of three biological replicates are combined, red bars represent the mean (Mann-Whitney test ****P<0,0001).
(C) WB analysis of the experiment depicted in **(A)**. Proteins MW is indicated in kDa. WB is representative of three independent replicates.
(D-E) Representative IF images of HeLa cells synchronized in mitosis using STLC and transfected with siNT or siPLK1 **(D)** and quantification of the relative UBAP2L intensity at kinetochores (arbitrary units A.U.) **(E)**. Regions of interest (ROIs) are shown in the corresponding numbered panels. Scale bar, 5µm. At least 50 cells were quantified per condition for each experiment. Each dot represents UBAP2L/CREST intensity ratio at a single pair of kinetochores. The measurements of three biological replicates are combined, red bars represent the mean (Mann-Whitney test ****P<0,0001).
(F) WB analysis of the experiment depicted in **(D)**. Proteins MW is indicated in kDa. WB is representative of three independent replicates.

Fig. 7. UBAP2L localizes to kinetochores before anaphase onset.

(A-B) Representative IF images of HeLa cells synchronized in mitosis using Monastrol and released for 0h, 45min or 1h30 to visualize all mitotic stages **(A)** and quantification of the relative UBAP2L recruitment to kinetochores (arbitrary units A.U.) **(B)**. ROIs are shown in the corresponding numbered panels. Scale bar, 5µm. At least 50 cells were quantified per cell cycle stage for each experiment. Each dot represents UBAP2L/CREST overlapping area at a single pair of kinetochores. The measurements of three biological replicates are combined, red bars represent the mean (Kruskal-Wallis test with Dunn's correction ****P<0,0001).
(C) Representative IF pictures of HeLa cells synchronized in mitosis using STLC and transfected with the indicated UBAP2L flag-tagged constructs. ROIs are shown in the corresponding numbered panels. Scale bar, 5µm.

Fig. 8. UBAP2L removes PLK1 from kinetochores.
(A-C) Representative IF images of control (siNT) or UBAP2L-downregulated cells synchronized in prometaphase using monastrol and released at the indicated time points. Scale bar, 5µm. Quantification of the percentage of cells expressing PLK1 **(B)** and of telophase cells with PLK1 at kinetochores **(C)**. At least 250 cells per condition were quantified for each replicate. Graphs represent the mean of three replicates ± SD (two sample two-tailed t-test or one-way ANOVA with Dunnett's correction **P<0,01, ***P<0,001, ****P<0,0001, ns=non-significant).
(D) WB analysis of WT or UBAP2L KO HeLa cells lysates after monastrol release at the indicated time points. Proteins MW is indicated in kDa. WB is representative of three independent replicates.
(E) Spinning disk time-lapse microscopy of PLK1-eGFP Knock-In (KI) HeLa cells synchronized with DTBR in mitosis. The selected frames of the movies are depicted and the corresponding time is indicated in minutes. SiR-DNA was used for DNA staining. Scale bar, 8µm.

Fig. 9. UBAP2L may regulate interaction of PLK1 with CUL3 to ensure faithful chromosome segregation.
(A) WB analysis of endogenous immunoprecipitation (IP) of IgG or UBAP2L from HeLa cells synchronized in mitosis using STLC. Proteins MW is indicated in kDa. WB is representative of three independent replicates.
(B) WB analysis of endogenous IP of IgG or PLK1 from HeLa control or UBAP2L-downregulated cells synchronized in mitosis using STLC. Proteins MW is indicated in kDa. WB is representative of three independent replicates.
(C) WB analysis of IP under denaturing conditions of WT or UBAP2L KO HeLa cells transiently transfected with plasmids encoding for GFP-PLK1 and His-Ubiquitin. The short exposure (s.e.) and long exposure (l.e.) of the membrane blotted against the FK2 antibody that specifically recognizes conjugated but not free ubiquitin are shown. Proteins MW is indicated in kDa. WB is representative of three independent replicates.
(D) WB analysis of control (siNT) or siUBAP2L treated HeLa cells were synchronized with monastrol, treated with DMSO or with 10nM of the PLK1 inhibitor BI2536 for 45min and

subsequently washed out from monastrol. Proteins MW is indicated in kDa. WB is representative of three independent replicates.

(E-H) DAPI staining of the experiment described in **(D)** showing different mitotic stages **(E)**. Quantification of the percentage of cells with misalignments **(F)**, DNA bridges **(G)** and micronuclei **(H)**. At least 100 cells from each mitotic stage were quantified for all conditions. Graphs represent the mean of three replicates ± SD (one-way ANOVA with Sidak's correction *P<0,05, **P<0,01, ***P<0,001, ****P<0,0001, ns=non-significant).

Materials and Methods

Antibodies

Primary antibodies used in this study are listed in Table S1 in the Supplementary Material file. Secondary antibodies used are the following: goat anti-mouse Alexa Fluor 488, goat anti-rabbit Alexa Fluor 488, goat anti-mouse Alexa Fluor 568, goat anti-rabbit Alexa Fluor 568, goat anti-human Alexa Fluor 568 (Thermo Scientific), goat anti-rabbit IgG-HRP conjugate and goat anti-mouse IgG-HRP conjugate (Biorad).

Generation of stable cell lines and cell culture

HeLa WT and UBAP2L KO cell lines were generated using CRISPR/Cas9-mediated gene editing as described in (Figure S1C). Two gRNAs targeting UBAP2L were cloned into pX330-P2A-EGFP/RFP (Zhang et al., 2017) through ligation using T4 ligase (New England Biolabs). HeLa cells were transfected and GFP and RFP double positive cells were collected by FACS (BD FACS Aria II), cultured for 2 days and seeded with FACS into 96-well plates. Obtained UBAP2L KO single-cell clones were validated by Western blot and sequencing of PCR-amplified targeted fragment by Sanger sequencing (GATC).

For the generation of PLK1-eGFP KI cell line, HeLa Kyoto cells were transfected with Cas9-eGFP, sgRNA 5'-TCGGCCAGCAACCGTCTCA-3' (targeting Plk1) and a repair templates (Genewiz). The repair template was designed as a fusion of 5xGly-eGFP flanked by two 500 bp arms, homologous to the genomic region around the Cas9 cutting site. 5 days after transfection eGFP positive cells were sorted and expanded for one week before a second sorting of single cells in a 96 well plates. After 2-3 weeks cells were screened by PCR.

All cultured cells were kept in culture in 5% CO2 humidified incubator at 37°C. HeLa Kyoto and derived stable cell lines (UBAP2L WT and KO, PLK1-eGFP KI) cell lines were cultured in Dulbecco's Modified Eagle Medium (DMEM 4,5g/L Glucose) supplemented with 10% Foetal Calf Serum (FCS), 1% penicillin and 1% streptomycin. Human U-2 Osteosarcoma (U2OS) cells were cultured in DMEM supplemented with 1g/L Glucose, 10% FCS and 40µg/mL Gentamycin. DLD-1 cells were kept in culture in Roswell Park Memorial Institute (RPMI) medium without HEPES supplemented with 10% FCS and 40µg/mL Gentamycin.

Cloning

Human UBAP2L isoform1 of 1087aa was isolated from HeLa cDNA and amplified by PCR. UBAP2L NT and CT fragments were generated using the primers listed in Table S2 in the Supplementary Material file. PCR products were cloned into pcDNA3.1 vector.

Plasmid and siRNA transfections

Lipofectamine RNAiMAX (Invitrogen) was used to transfect siRNAs according to the manufacturer's instructions. Final concentration of siRNA used varies from 20 to 40nM. All used oligonucleotides are listed in the key resources table.

Jetpei (Polyplus transfection) or X-tremeGENE9 (Roche) DNA transfection reagents were used to perform plasmid transfections.

Cell synchronization

Cell cycle synchronization in G1/S, S or G2 phases was performed as previously described (Agote-Arán et al., 2021). For synchronization in mitosis, cells were incubated in the presence of 1µM Taxol (Sigma), 1mM Monastrol (Euromedex) or 5µM STLC (Enzolifesciences) for 16h. For monastrol washout experiments, cells were collected and centrifuged at 1500rpm for 5min and resuspended in warm medium. This procedure was repeated three times and cells were cultured and collected at the desired timepoint post-release.

Cell treatments

In order to inhibit translation, cells were treated with 100µg/mL CHX (Sigma) for the indicated time. To inhibit proteasomal degradation, cells were treated with 25µM MG132 (Tocris bioscience) for the indicated time. PLK1 enzymatic activity was inhibited using 10nM BI2536 (Euromedex) for 45min.

Western Blotting (WB)

Cells were collected by centrifugation at 1500rpm for 5 min at 4°C and washed three times with cold 1X PBS. Cell pellets were lysed using 1X RIPA buffer (50 mM Tris-HCl pH 7.5, 150 mM NaCl, 1% Triton X-100, 1 mM EDTA, 1 mM EGTA, 2 mM Sodium pyrophosphate, 1 mM NaVO4 (Na3O4V) and 1 mM NaF) supplemented with protease inhibitor cocktail (Roche) and incubated on ice for 30 min with periodic vortexing. After centrifugation at 14 000rpm for 30 min at 4 ºC, total protein concentration was measured using Bradford assay by Bio-Rad Protein Assay kit (Bio-Rad). Samples were boiled for 10 min at 96 °C in 1X Laemmli buffer (LB) with β-Mercaptoethanol (BioRad) and resolved on pre-cast 4-12% Bis-Tris gradient gels (Thermo Scientific) before being transferred to a polyvinylidene difluoride (PVDF) membrane (Millipore) using wet transfer modules (BIO-RAD Mini-PROTEAN® Tetra System). Membranes were blocked in 5% non-fat milk powder, 5% bovine serum albumin (BSA, Millipore), or 5% non-fat milk powder mixed with 3% BSA for 1h at room temperature, followed by incubation with antibodies diluted in TBS-T-5% BSA/5% milk. All incubations with primary antibodies were performed for overnight at 4°C.

Membranes were washed with TBS-T and developed using Luminata Forte Western HRP substrate (Merck Millipore).

Immunoprecipitations (IPs)

Cells were collected by centrifugation at 1500rpm for 5min at 4°C and washed twice with ice-cold 1X PBS and cell lysates for immunoprecipitation were prepared using IP buffer (25 mM Tris-HCl pH7.5, 150 mM NaCl, 1% Triton X-100, 5mM MgCl2, 2mM EDTA, 2mM PMSF and 10mM NaF) supplemented with protease inhibitors (Roche) and incubated on ice for 20 minutes. After centrifugation at 14000rpm for 30 minutes at 4°C cleared supernatant was used immediately. Lysates were equilibrated to volume and concentration.

For endogenous IPs, IgG and target specific antibodies (anti-UBAP2L or anti-PLK1) as well as protein G sepharose 4 Fast Flow beads (GE Healthcare Life Sciences) were used. Samples were incubated with the IgG and specific antibodies overnight at 4°C under rotation. Beads were blocked with 3% BSA diluted in 1X IP buffer and incubated for 4h at 4°C with rotation. Next, the IgG/specific antibodies-samples and blocked beads were incubated together to a final volume of 1 ml for 4h at 4°C under rotation. The beads were washed with IP buffer 4 to 6 times for 10 min each at 4°C under rotation. Notably, beads were pelleted by centrifugation at 1500rpm for 5 min at 4°C. The washed beads were directly eluted in 2X LB with β-Mercaptoethanol and boiled for 10 min at 96°C and samples were resolved by WB as described above.

For IP under denaturing conditions, HeLa cells were transfected with His/Biotin Ubiquitin and pEGFP-PLK1 or with His/Biotin Ubiquitin and pEGFP-N1 for 30h. Cells were treated with 50μM MG132 and lysed in Urea lysis buffer (8M Urea, 300mM NaCl, 50mM Na2HPO4, 50mM Tris-HCl and 1mM PMSF, pH8). Supernatants were cleared by centrifugation at 14000rpm for 15 minutes and incubated with GFP-Trap agarose beads (Chromotek) overnight at 4°C under rotation. Beads were washed by Urea lysis buffer, eluted in 2X LB and analyzed by WB.

Subcellular fractionation

After appropriate cell synchronization, cells were collected by centrifugation at 1500rpm for 5min at 4°C. The cytosolic fraction was removed by incubation in hypotonic buffer (10mM HEPES pH7, 50mM NaCl, 0,3M sucrose, 0,5% Triton X-100) supplemented with protease inhibitors cocktail (Roche) for 10min on ice and centrifuged at 1500rpm for 5min at 4°C. The remaining pellet was washed with the washing buffer (10mM HEPES pH7, 50mM NaCl, 0,3M sucrose) supplemented with protease inhibitors cocktail (Roche). The soluble nuclear fraction was collected by incubation with the nuclear buffer (10mM HEPES pH7, 200mM NaCl, 1mM EDTA, 0,5% NP-40) supplemented with protease inhibitors cocktail (Roche) for 10min on ice and centrifuge at 14000rpm for 2min at 4°C. Lysates were boiled for 10 min at 96 °C in 1X LB with β-Mercaptoethanol (BioRad) and analyzed by WB.

Immunofluorescence

Mitotic cells were collected with cell scrapers, centrifuged on Thermo Scientific Shandon Cytospin 4 Cytocentrifuge for 5 minutes at 1000 rpm and fixed with 4% PFA for 10 min at room temperature. Interphasic cells were cultured directly on coverslips, collected and fixed with 4% PFA for 10 min at room temperature. Cells were washed 3 times with 1X PBS and permeabilized with 0.5% NP-40 for 5min, rinsed with PBS-Triton 0.01% (PBS-T) and blocked with 3% BSA for 1h. Cells were then incubated with primary antibodies in blocking buffer for 1h at room temperature, washed 3 times with PBS-T and incubated with secondary antibodies in blocking buffer for 45 min at room temperature in the dark. After incubation, cells were washed 3 times with PBS-T and glass coverslips were added on cells (mitosis) or coverslips were mounted onto slides with Mowiol containing DAPI (Calbiochem).

Live-imaging microscopy

For live-cell microscopy, cells were grown on 35mm glass bottom dishes with four compartments and SiR-DNA (Spirochrom) was added 1h before filming. For the experiment described in Figure 1, cells were synchronized with Double Thymidine and Release (DTBR) protocol and were filmed 8h after release using a 63x water immersion objective for a total time frame of 8h. The acquisition was done by the Yokogawa W1 rotating disk combined with a Leica 63x/1.0 water lens. For the experiments described in Figure 6, HeLa GFP-PLK1 KI cells were synchronized using DTBR protocol and were filmed 10h after release for a total time frame of 8h. Images were acquired every 10 min in stacks of 12µm range (0,5µm steps). Image analysis was performed using ImageJ software.

Colony formation assay

Colony Formation Assay was performed as previously described (Pangou et al., 2021). Briefly, 500 cells were plated per well in a 6-well plate in technical triplicate for each condition and were cultures for 7 days. Colonies were washed using 1X PBS and fixed with 4% paraformaldehyde (PFA) and stained with 0,1% Crystal Violet for 30min. The number of colonies and individual area were counted using an automated pipeline generated on Fiji software. Three biological replicates were performed.

Automatic nuclear intensity measurements

Quantification of nuclear intensity was conducted using CellProfiler as previously described (Agote-Aran et al., 2020). Briefly, the DAPI channel of pictures was used to delimit the area of interest (nucleus) and intensity of the desired channel was automatically measured in this specific area. At least 200 cells from three biological replicates were measured per condition.

Statistical analysis

At least three independent biological replicates were performed for each experiment. Graphs were made using GraphPad Prism and Adobe illustrator softwares. Schemes were created using

BioRender.com. All experiments were done in a strictly double-blind manner. Image quantifications were carried out in a blinded manner. Normal distribution was assessed using Shapiro-Wilk test for each experiment. Normal sets of data were analyzed using two sample two-tailed T-test or One-way ANOVA with Dunnett's or Sidak's correction in case of multiple group analysis. For non-normal data, Mann-Whitney's or Kruskal-Wallis test with Dunn's correction tests were performed. Graphically, error bars represent Standard Deviation (SD) and for all experiments, significance stars were assigned as following: * P<0,05, ** P<0,01, *** P<0,001, **** P<0,0001, ns=non-significant.

References

Agote-Arán, A., J. Lin, and I. Sumara. 2021. Fragile X-Related Protein 1 Regulates Nucleoporin Localization in a Cell Cycle-Dependent Manner. *Front Cell Dev Biol*. 9:755847. doi:10.3389/fcell.2021.755847.

Agote-Aran, A., S. Schmucker, K. Jerabkova, I. Jmel Boyer, A. Berto, L. Pacini, P. Ronchi, C. Kleiss, L. Guerard, Y. Schwab, H. Moine, J.-L. Mandel, S. Jacquemont, C. Bagni, and I. Sumara. 2020. Spatial control of nucleoporin condensation by fragile X-related proteins. *EMBO J*. 39:e104467. doi:10.15252/embj.2020104467.

Akopian, D., C.A. McGourty, and M. Rapé. 2022. Co-adaptor driven assembly of a CUL3 E3 ligase complex. *Molecular Cell*. 82:585-597.e11. doi:10.1016/j.molcel.2022.01.004.

Barr, F.A., H.H.W. Silljé, and E.A. Nigg. 2004. Polo-like kinases and the orchestration of cell division. *Nat. Rev. Mol. Cell Biol.* 5:429–440. doi:10.1038/nrm1401.

Beck, J., S. Maerki, M. Posch, T. Metzger, A. Persaud, H. Scheel, K. Hofmann, D. Rotin, P. Pedrioli, J.R. Swedlow, M. Peter, and I. Sumara. 2013. Ubiquitylation-dependent localization of PLK1 in mitosis. *Nat Cell Biol*. 15:430–439. doi:10.1038/ncb2695.

Bennett, E.J., J. Rush, S.P. Gygi, and J.W. Harper. 2010. Dynamics of cullin-RING ubiquitin ligase network revealed by systematic quantitative proteomics. *Cell*. 143:951–65. doi:10.1016/j.cell.2010.11.017.

Bruinsma, W., J.A. Raaijmakers, and R.H. Medema. 2012. Switching Polo-like kinase-1 on and off in time and space. *Trends Biochem. Sci.* 37:534–542. doi:10.1016/j.tibs.2012.09.005.

Cheng, B., and K. Crasta. 2017. Consequences of mitotic slippage for antimicrotubule drug therapy. *Endocr. Relat. Cancer*. 24:T97–T106. doi:10.1530/ERC-17-0147.

Chiappa, M., S. Petrella, G. Damia, M. Broggini, F. Guffanti, and F. Ricci. 2022. Present and Future Perspective on PLK1 Inhibition in Cancer Treatment. *Front Oncol*. 12:903016. doi:10.3389/fonc.2022.903016.

Cirillo, L., A. Cieren, S. Barbieri, A. Khong, F. Schwager, R. Parker, and M. Gotta. 2020. UBAP2L Forms Distinct Cores that Act in Nucleating Stress Granules Upstream of G3BP1. *Current Biology*. 30:698-707.e6. doi:10.1016/j.cub.2019.12.020.

Combes, G., I. Alharbi, L.G. Braga, and S. Elowe. 2017. Playing polo during mitosis: PLK1 takes the lead. *Oncogene*. 36:4819–4827. doi:10.1038/onc.2017.113.

Courtheoux, T., R.I. Enchev, F. Lampert, J. Gerez, J. Beck, P. Picotti, I. Sumara, and M. Peter. 2016. Cortical dynamics during cell motility are regulated by CRL3KLHL21 E3 ubiquitin ligase. *Nat Commun*. 7:12810. doi:10.1038/ncomms12810.

Dephoure, N., C. Zhou, J. Villén, S.A. Beausoleil, C.E. Bakalarski, S.J. Elledge, and S.P. Gygi. 2008. A quantitative atlas of mitotic phosphorylation. *Proc Natl Acad Sci U S A*. 105:10762–10767. doi:10.1073/pnas.0805139105.

Elowe, S., S. Hummer, A. Uldschmid, X. Li, and E.A. Nigg. 2007. Tension-sensitive Plk1 phosphorylation on BubR1 regulates the stability of kinetochore microtubule interactions. *Genes Dev*. 21:2205–19. doi:10.1101/gad.436007.

Fairley, J.A., L.E. Mitchell, T. Berg, N.S. Kenneth, C. von Schubert, H.H.W. Silljé, R.H. Medema, E.A. Nigg, and R.J. White. 2012. Direct regulation of tRNA and 5S rRNA gene transcription by Polo-like kinase 1. *Mol Cell*. 45:541–552. doi:10.1016/j.molcel.2011.11.030.

Fournier, M., M. Orpinell, C. Grauffel, E. Scheer, J.-M. Garnier, T. Ye, V. Chavant, M. Joint, F. Esashi, A. Dejaegere, P. Gönczy, and L. Tora. 2016. KAT2A/KAT2B-targeted acetylome reveals a role for PLK4 acetylation in preventing centrosome amplification. *Nat Commun*. 7:13227. doi:10.1038/ncomms13227.

Golsteyn, R.M., K.E. Mundt, A.M. Fry, and E.A. Nigg. 1995. Cell cycle regulation of the activity and subcellular localization of Plk1, a human protein kinase implicated in mitotic spindle function. *Journal of Cell Biology*. 129:1617–1628. doi:10.1083/jcb.129.6.1617.

Goto, H., T. Kiyono, Y. Tomono, A. Kawajiri, T. Urano, K. Furukawa, E.A. Nigg, and M. Inagaki. 2006. Complex formation of Plk1 and INCENP required for metaphase-anaphase transition. *Nat. Cell Biol.* 8:180–187. doi:10.1038/ncb1350.

Guerber, L., E. Pangou, and I. Sumara. 2022. Ubiquitin Binding Protein 2-Like (UBAP2L): is it so NICE After All? *Front Cell Dev Biol*. 10:931115. doi:10.3389/fcell.2022.931115.

Gulino, A., L. Di Marcotullio, and I. Screpanti. 2010. The multiple functions of Numb. *Exp Cell Res*. 316:900–906. doi:10.1016/j.yexcr.2009.11.017.

Gutteridge, R.E.A., M.A. Ndiaye, X. Liu, and N. Ahmad. 2016. Plk1 Inhibitors in Cancer Therapy: From Laboratory to Clinics. *Mol Cancer Ther*. 15:1427–1435. doi:10.1158/1535-7163.MCT-15-0897.

Herlihy, A.E., S. Boeing, J.C. Weems, J. Walker, A.B. Dirac-Svejstrup, M.H. Lehner, R.C. Conaway, J.W. Conaway, and J.Q. Svejstrup. 2022. UBAP2/UBAP2L regulate UV-induced ubiquitylation of RNA polymerase II and are the human orthologues of yeast Def1. *DNA Repair (Amst)*. 115:103343. doi:10.1016/j.dnarep.2022.103343.

Huang, C., Y. Chen, H. Dai, H. Zhang, M. Xie, H. Zhang, F. Chen, X. Kang, X. Bai, and Z. Chen. 2020. UBAP2L arginine methylation by PRMT1 modulates stress granule assembly. *Cell Death Differ*. 27:227–241. doi:10.1038/s41418-019-0350-5.

Jang, S.-M., C.E. Redon, B.L. Thakur, M.K. Bahta, and M.I. Aladjem. 2020. Regulation of cell cycle drivers by Cullin-RING ubiquitin ligases. *Exp Mol Med*. 52:1637–1651. doi:10.1038/s12276-020-00508-4.

Jerabkova, K., and I. Sumara. 2019. Cullin 3, a cellular scripter of the non-proteolytic ubiquitin code. *Seminars in Cell & Developmental Biology*. 93:100–110. doi:10.1016/j.semcdb.2018.12.007.

Jevtić, P., L.J. Edens, L.D. Vuković, and D.L. Levy. 2014. Sizing and shaping the nucleus: mechanisms and significance. *Curr Opin Cell Biol*. 28:16–27. doi:10.1016/j.ceb.2014.01.003.

Jiang, N., X. Wang, M. Jhanwar-Uniyal, Z. Darzynkiewicz, and W. Dai. 2006. Polo Box Domain of Plk3 Functions as a Centrosome Localization Signal, Overexpression of Which Causes Mitotic Arrest, Cytokinesis Defects, and Apoptosis. *Journal of Biological Chemistry*. 281:10577–10582. doi:10.1074/jbc.M513156200.

Krupina, K., A. Goginashvili, and D.W. Cleveland. 2021. Causes and consequences of micronuclei. *Curr Opin Cell Biol*. 70:91–99. doi:10.1016/j.ceb.2021.01.004.

Krupina, K., C. Kleiss, T. Metzger, S. Fournane, S. Schmucker, K. Hofmann, B. Fischer, N. Paul, I.M. Porter, W. Raffelsberger, O. Poch, J.R. Swedlow, L. Brino, and I. Sumara. 2016. Ubiquitin Receptor Protein UBASH3B Drives Aurora B Recruitment to Mitotic Microtubules. *Dev Cell*. 36:63–78. doi:10.1016/j.devcel.2015.12.017.

Kumar, S., G. Sharma, C. Chakraborty, A.R. Sharma, and J. Kim. 2017. Regulatory functional territory of PLK-1 and their substrates beyond mitosis. *Oncotarget*. 8:37942–37962. doi:10.18632/oncotarget.16290.

Lenart, P., M. Petronczki, M. Steegmaier, B. Di Fiore, J.J. Lipp, M. Hoffmann, W.J. Rettig, N. Kraut, and J.M. Peters. 2007. The small-molecule inhibitor BI 2536 reveals novel insights into mitotic roles of polo-like kinase 1. *Curr Biol*. 17:304–15. doi:10.1016/j.cub.2006.12.046.

Lera, R.F., G.K. Potts, A. Suzuki, J.M. Johnson, E.D. Salmon, J.J. Coon, and M.E. Burkard. 2016. Decoding Polo-like kinase 1 signaling along the kinetochore–centromere axis. *Nat Chem Biol*. 12:411–418. doi:10.1038/nchembio.2060.

Lindon, C., and J. Pines. 2004. Ordered proteolysis in anaphase inactivates Plk1 to contribute to proper mitotic exit in human cells. *Journal of Cell Biology*. 164:233–241. doi:10.1083/jcb.200309035.

Liu, D., O. Davydenko, and M.A. Lampson. 2012. Polo-like kinase-1 regulates kinetochore-microtubule dynamics and spindle checkpoint silencing. *J Cell Biol*. 198:491–9. doi:10.1083/jcb.201205090.

Maeda, M., H. Hasegawa, M. Sugiyama, T. Hyodo, S. Ito, D. Chen, E. Asano, A. Masuda, Y. Hasegawa, M. Hamaguchi, and T. Senga. 2016. Arginine methylation of ubiquitin-associated protein 2-like is required for the accurate distribution of chromosomes. *FASEB J*. 30:312–323. doi:10.1096/fj.14-268987.

Maerki, S., M.H. Olma, T. Staubli, P. Steigemann, D.W. Gerlich, M. Quadroni, I. Sumara, and M. Peter. 2009. The Cul3-KLHL21 E3 ubiquitin ligase targets aurora B to midzone microtubules in anaphase and is required for cytokinesis. *J Cell Biol*. 187:791–800. doi:10.1083/jcb.200906117.

Maia, A.R., Z. Garcia, L. Kabeche, M. Barisic, S. Maffini, S. Macedo-Ribeiro, I.M. Cheeseman, D.A. Compton, I. Kaverina, and H. Maiato. 2012. Cdk1 and Plk1 mediate a CLASP2 phospho-switch that stabilizes kinetochore-microtubule attachments. *J Cell Biol*. 199:285–301. doi:10.1083/jcb.201203091.

McIntosh, J.R. 2016. Mitosis. *Cold Spring Harb Perspect Biol*. 8:a023218. doi:10.1101/cshperspect.a023218.

McKinley, K.L., and I.M. Cheeseman. 2014. Polo-like Kinase 1 Licenses CENP-A Deposition at Centromeres. *Cell*. 158:397–411. doi:10.1016/j.cell.2014.06.016.

Moghe, S., F. Jiang, Y. Miura, R.L. Cerny, M.-Y. Tsai, and M. Furukawa. 2012. The CUL3-KLHL18 ligase regulates mitotic entry and ubiquitylates Aurora-A. *Biology Open*. 1:82–91. doi:10.1242/bio.2011018.

Nigg, E.A. 2001. Mitotic kinases as regulators of cell division and its checkpoints. *Nat Rev Mol Cell Biol*. 2:21–32. doi:10.1038/35048096.

Pangou, E., O. Bielska, L. Guerber, S. Schmucker, A. Agote-Arán, T. Ye, Y. Liao, M. Puig-Gamez, E. Grandgirard, C. Kleiss, Y. Liu, E. Compe, Z. Zhang, R. Aebersold, R. Ricci, and I. Sumara. 2021. A PKD-MFF signaling axis couples mitochondrial fission to mitotic progression. *Cell Rep*. 35:109129. doi:10.1016/j.celrep.2021.109129.

Parrilla, A., L. Cirillo, Y. Thomas, M. Gotta, L. Pintard, and A. Santamaria. 2016. Mitotic entry: The interplay between Cdk1, Plk1 and Bora. *Cell Cycle*. 15:3177–3182. doi:10.1080/15384101.2016.1249544.

Petronczki, M., P. Lenart, and J.M. Peters. 2008. Polo on the Rise-from Mitotic Entry to Cytokinesis with Plk1. *Dev Cell*. 14:646–59. doi:10.1016/j.devcel.2008.04.014.

Pines, J. 1997. Localization of cell cycle regulators by immunofluorescence. *In* Methods in Enzymology. Elsevier. 99–113.

Qi, W., Z. Tang, and H. Yu. 2006. Phosphorylation- and polo-box-dependent binding of Plk1 to Bub1 is required for the kinetochore localization of Plk1. *Mol. Biol. Cell*. 17:3705–3716. doi:10.1091/mbc.E06-03-0240.

Rai, A.K., J.-X. Chen, M. Selbach, and L. Pelkmans. 2018. Kinase-controlled phase transition of membraneless organelles in mitosis. *Nature*. 559:211–216. doi:10.1038/s41586-018-0279-8.

S. Pedersen, R., G. Karemore, T. Gudjonsson, M.-B. Rask, B. Neumann, J.-K. Hériché, R. Pepperkok, J. Ellenberg, D.W. Gerlich, J. Lukas, and C. Lukas. 2016. Profiling DNA damage response following mitotic perturbations. *Nat Commun*. 7:13887. doi:10.1038/ncomms13887.

Santamaria, A., B. Wang, S. Elowe, R. Malik, F. Zhang, M. Bauer, A. Schmidt, H.H.W. Silljé, R. Körner, and E.A. Nigg. 2011. The Plk1-dependent Phosphoproteome of the Early Mitotic Spindle. *Molecular & Cellular Proteomics*. 10:M110.004457. doi:10.1074/mcp.M110.004457.

Schmit, T.L., M. Nihal, M. Ndiaye, V. Setaluri, V.S. Spiegelman, and N. Ahmad. 2012. Numb regulates stability and localization of the mitotic kinase PLK1 and is required for transit through mitosis. *Cancer Res.* 72:3864–3872. doi:10.1158/0008-5472.CAN-12-0714.

Schmucker, S., and I. Sumara. 2014. Molecular dynamics of PLK1 during mitosis. *Mol Cell Oncol*. 1:e954507. doi:10.1080/23723548.2014.954507.

Strebhardt, K. 2010. Multifaceted polo-like kinases: drug targets and antitargets for cancer therapy. *Nat Rev Drug Discov*. 9:643–60. doi:10.1038/nrd3184.

Sugimoto, K., T. Urano, H. Zushi, K. Inoue, H. Tasaka, M. Tachibana, and M. Dotsu. 2002. Molecular Dynamics of Aurora-A Kinase in Living Mitotic Cells Simultaneously Visualized with Histone H3 and Nuclear Membrane Protein Importin.ALPHA.. *Cell Struct. Funct.* 27:457–467. doi:10.1247/csf.27.457.

Sumara, I., J.F. Gimenez-Abian, D. Gerlich, T. Hirota, C. Kraft, C. de la Torre, J. Ellenberg, and J.M. Peters. 2004. Roles of polo-like kinase 1 in the assembly of functional mitotic spindles. *Curr Biol*. 14:1712–22. doi:10.1016/j.cub.2004.09.049.

Sumara, I., M. Quadroni, C. Frei, M.H. Olma, G. Sumara, R. Ricci, and M. Peter. 2007. A Cul3-based E3 ligase removes Aurora B from mitotic chromosomes, regulating mitotic progression and completion of cytokinesis in human cells. *Dev Cell*. 12:887–900. doi:10.1016/j.devcel.2007.03.019.

Warnke, S., S. Kemmler, R.S. Hames, H.-L. Tsai, U. Hoffmann-Rohrer, A.M. Fry, and I. Hoffmann. 2004. Polo-like Kinase-2 Is Required for Centriole Duplication in Mammalian Cells. *Current Biology*. 14:1200–1207. doi:10.1016/j.cub.2004.06.059.

Yamagishi, Y., T. Honda, Y. Tanno, and Y. Watanabe. 2010. Two Histone Marks Establish the Inner Centromere and Chromosome Bi-Orientation. *Science*. 330:239–243. doi:10.1126/science.1194498.

Youn, J.-Y., W.H. Dunham, S.J. Hong, J.D.R. Knight, M. Bashkurov, G.I. Chen, H. Bagci, B. Rathod, G. MacLeod, S.W.M. Eng, S. Angers, Q. Morris, M. Fabian, J.-F. Côté, and A.-C. Gingras. 2018. High-Density Proximity Mapping Reveals the Subcellular Organization of mRNA-Associated Granules and Bodies. *Molecular Cell*. 69:517-532.e11. doi:10.1016/j.molcel.2017.12.020.

Zhang, Z., G. Meszaros, W. He, Y. Xu, H. de Fatima Magliarelli, L. Mailly, M. Mihlan, Y. Liu, M. Puig Gámez, A. Goginashvili, A. Pasquier, O. Bielska, B. Neven, P. Quartier, R. Aebersold, T.F. Baumert, P. Georgel, J. Han, and R. Ricci. 2017. Protein kinase D at the Golgi controls NLRP3 inflammasome activation. *Journal of Experimental Medicine*. 214:2671–2693. doi:10.1084/jem.20162040.

Zhuo, X., X. Guo, X. Zhang, G. Jing, Y. Wang, Q. Chen, Q. Jiang, J. Liu, and C. Zhang. 2015. Usp16 regulates kinetochore localization of Plk1 to promote proper chromosome alignment in mitosis. *J. Cell Biol.* 210:727–735. doi:10.1083/jcb.201502044.

Zitouni, S., C. Nabais, S.C. Jana, A. Guerrero, and M. Bettencourt-Dias. 2014. Polo-like kinases: structural variations lead to multiple functions. *Nat. Rev. Mol. Cell Biol.* 15:433–452. doi:10.1038/nrm3819.

Acknowledgments: We are grateful to Monica Gotta and Luca Cirillo from the Department of Cell Physiology and Metabolism and University of Geneva that kindly generated and shared with us the HeLa PLK1-eGFP knock in cell line, as well as for helpful discussions on the manuscript. We thank the Imaging Center of the IGBMC (ICI) and the IGBMC core facilities for their support on this research. L.G. was supported by Labex international PhD fellowship from IGBMC and IMC-Bio graduate school. E.P. was supported by postdoctoral fellowships from the ANR-10-LABX-0030-INRT. Research in the I.S. laboratory was supported by IGBMC, CNRS, Fondation ARC pour la recherche sur le cancer (ARC), Institut National du Cancer (INCa), Ligue Nationale contre le Cancer, USIAS and Sanofi iAward Europe. This work of the Interdisciplinary Thematic Institute IMCBio, as part of the ITI 2021-2028 program of the University of Strasbourg, CNRS and Inserm, was supported by IdEx Unistra (ANR-10-IDEX-0002), and by SFRI-STRAT'US project (ANR 20-SFRI-0012) and EUR IMCBio (ANR-17-EURE-0023) under the framework of the French Investments for the Future Program.

Author contributions: Conceptualization: E.P. and I.S., Software: E.G., Methodology: L.G. and E.P., Validation: L.G and E.P., Formal Analysis: L.G and E.P., Investigation: L.G., E.P., A.V., Y.L. and C.K., Writing-Original Draft: L.G., E.P. and I.S. Writing-Review and Editing: E.P., and I.S., Visualization: L.G., E.P., and I.S., Supervision: E.P. and I.S. Funding Acquisition: I.S.

Declaration of interests: The authors declare no competing interests.

Figure 1.

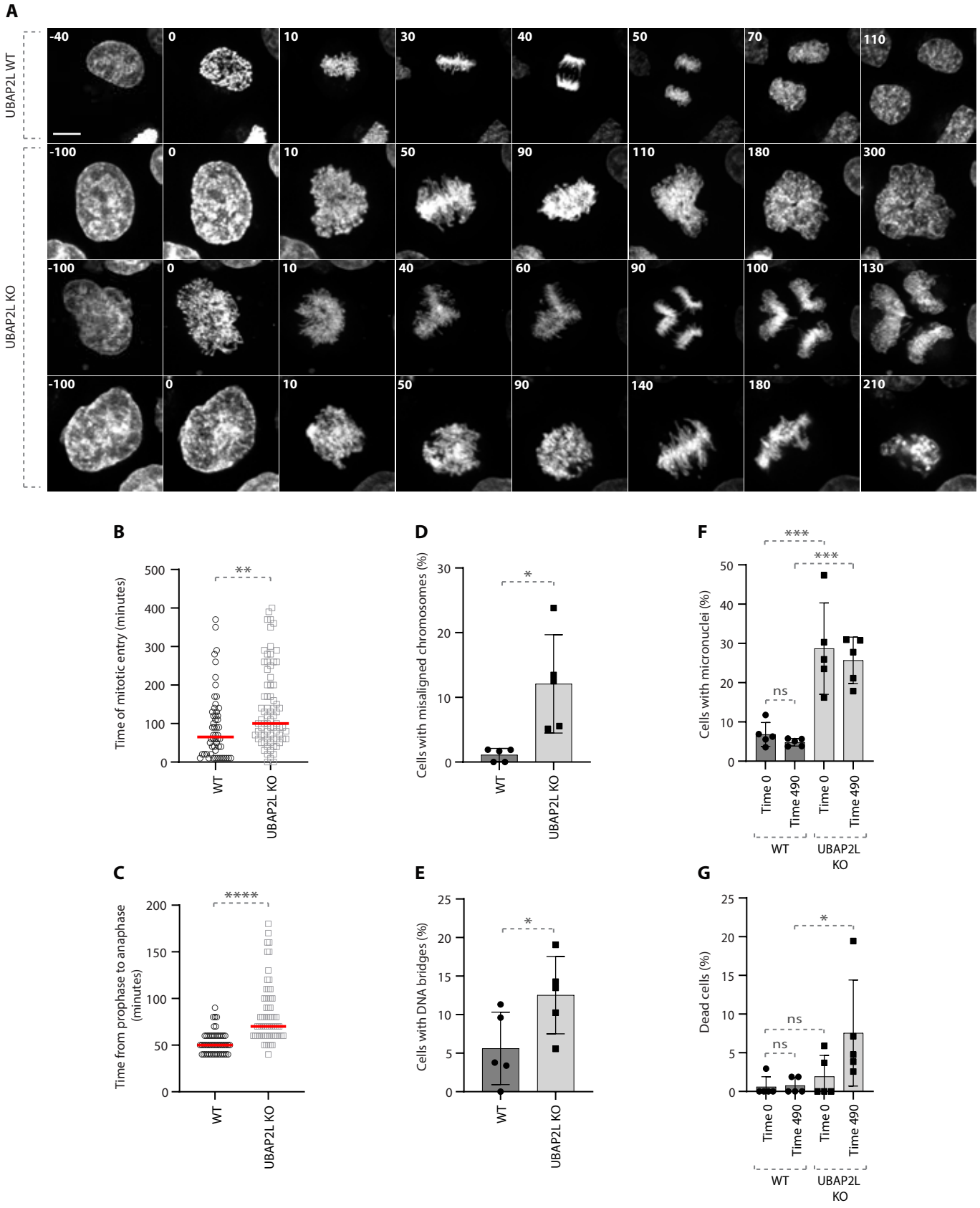

Figure 2.

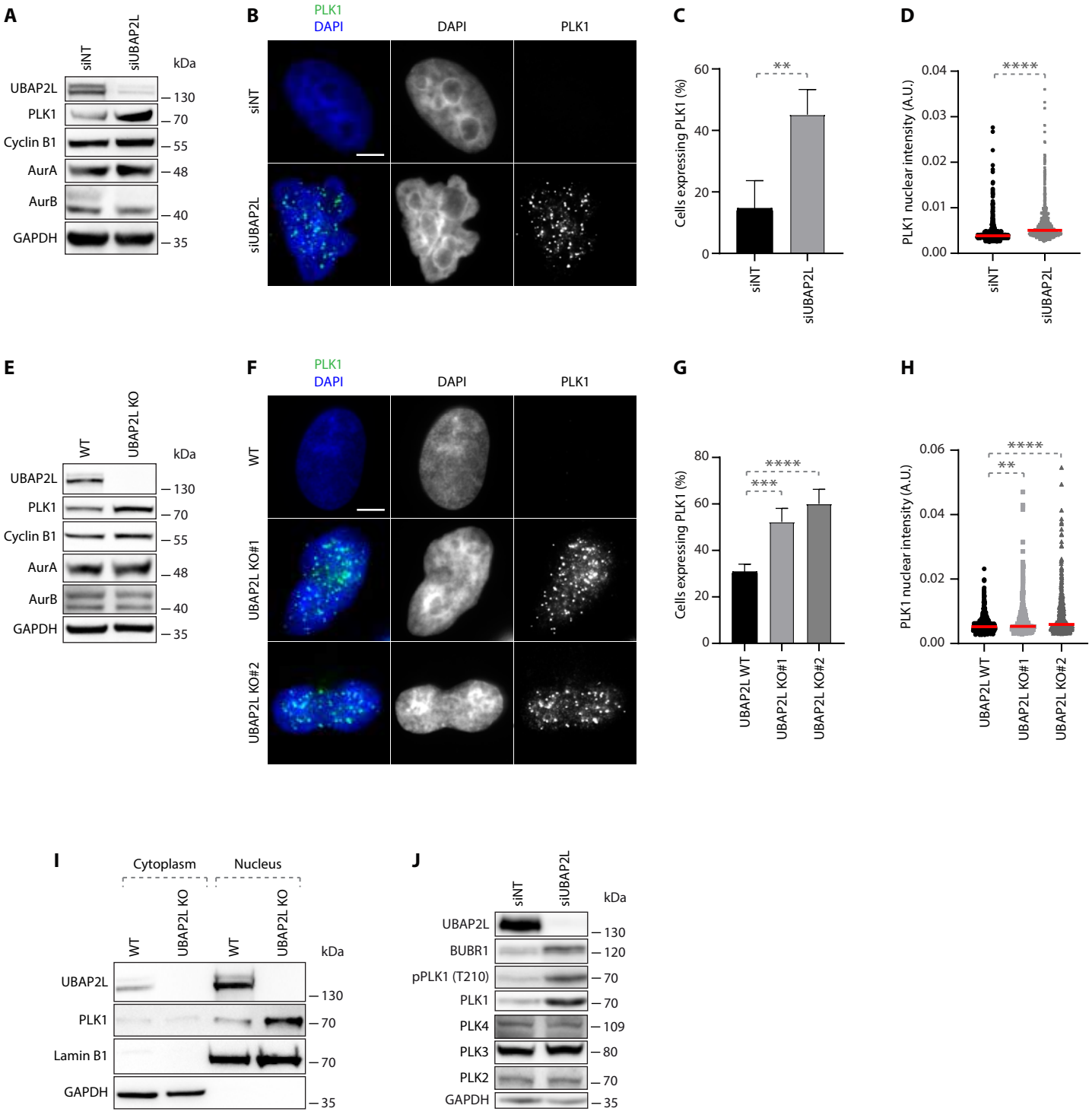

Figure 3.

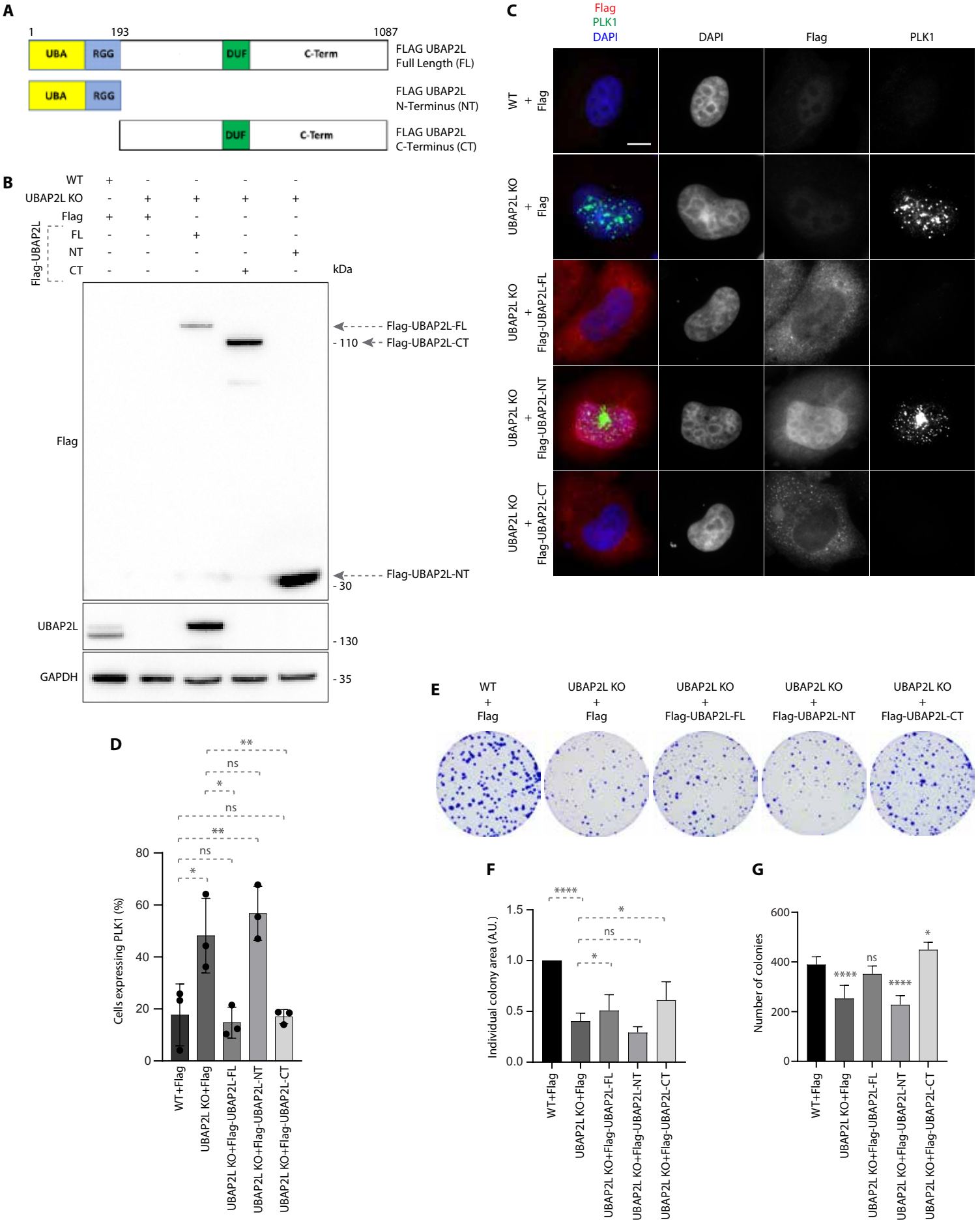

Figure 4.

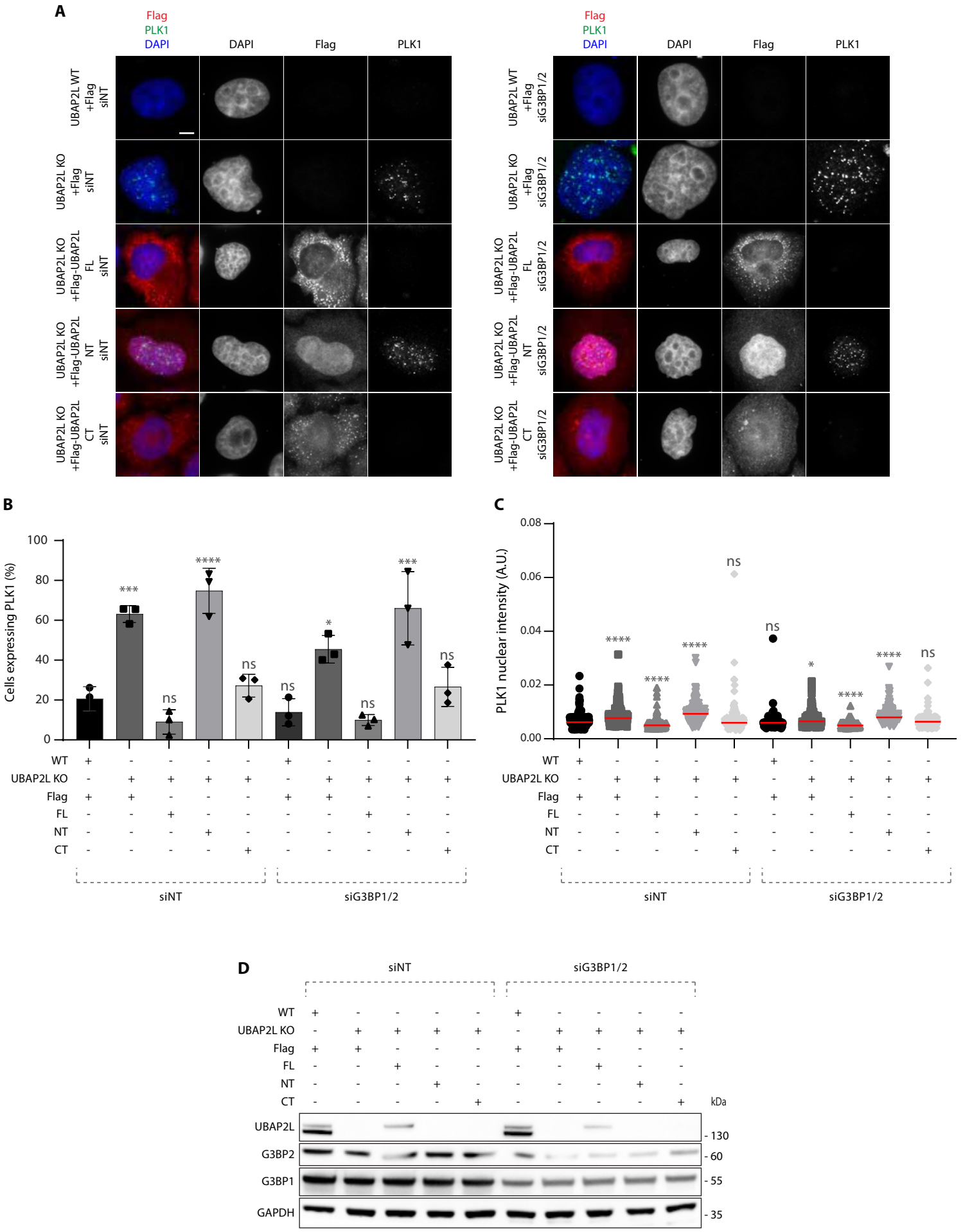

Figure 5.

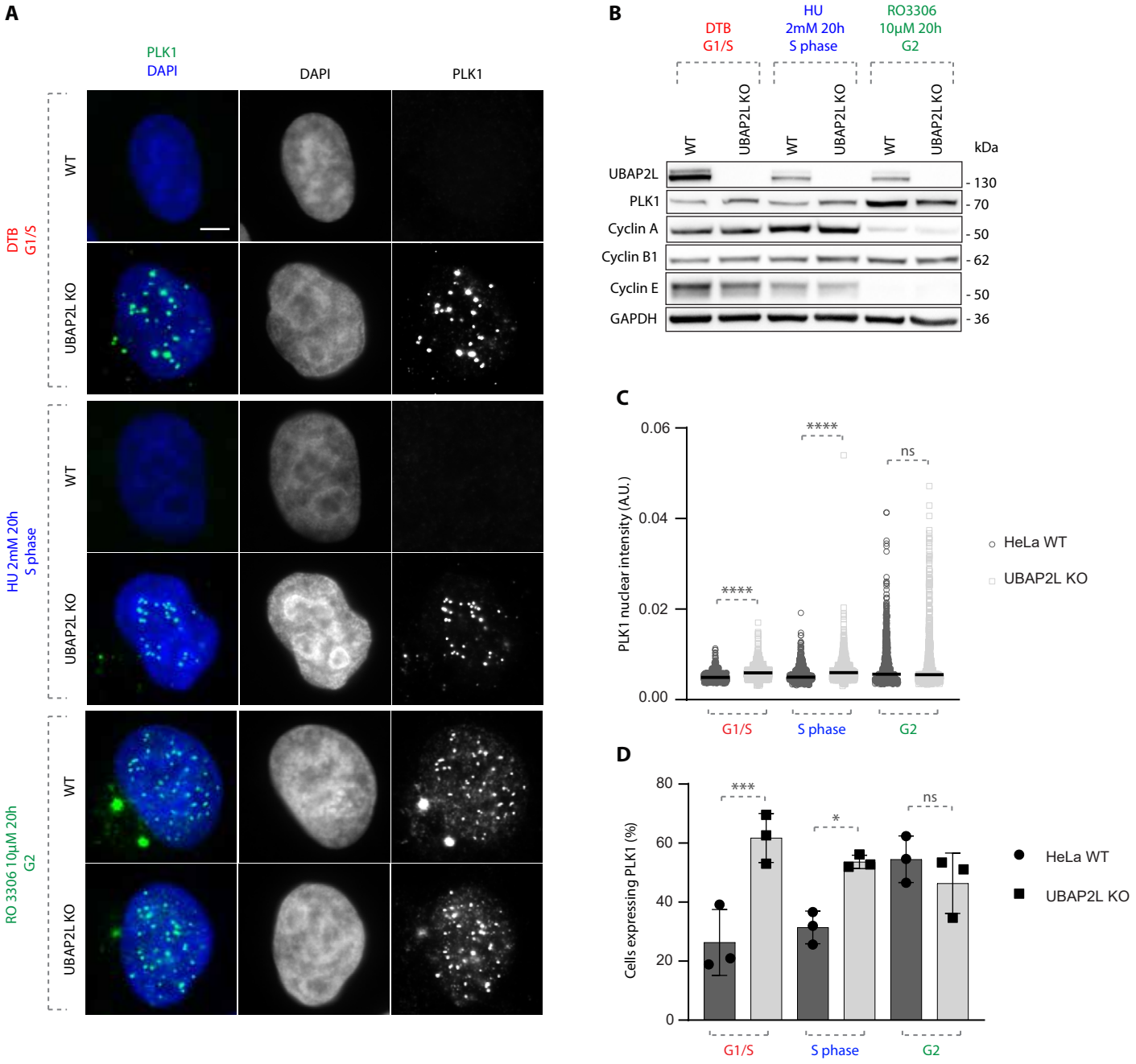

Figure 6.

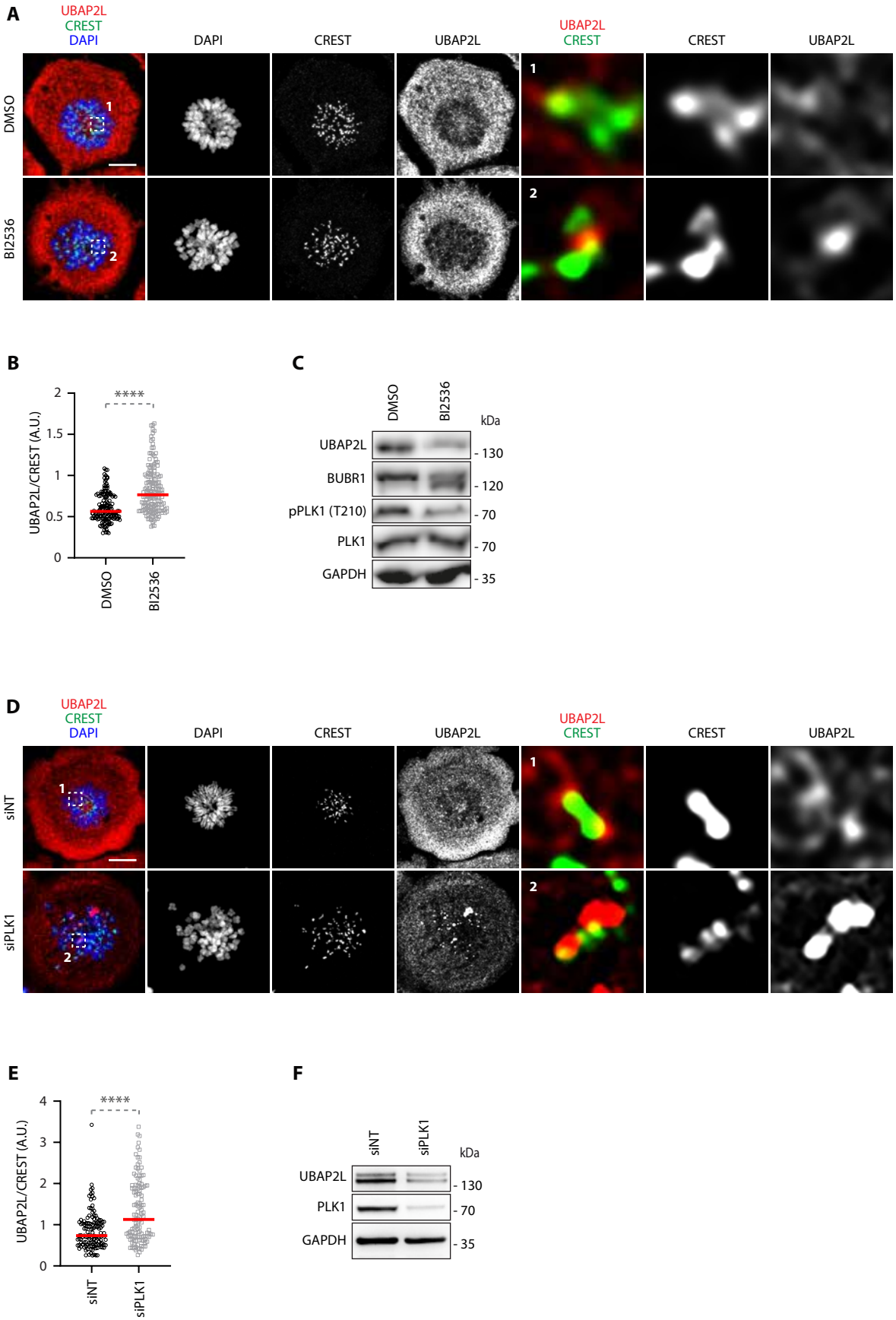

Figure 7.

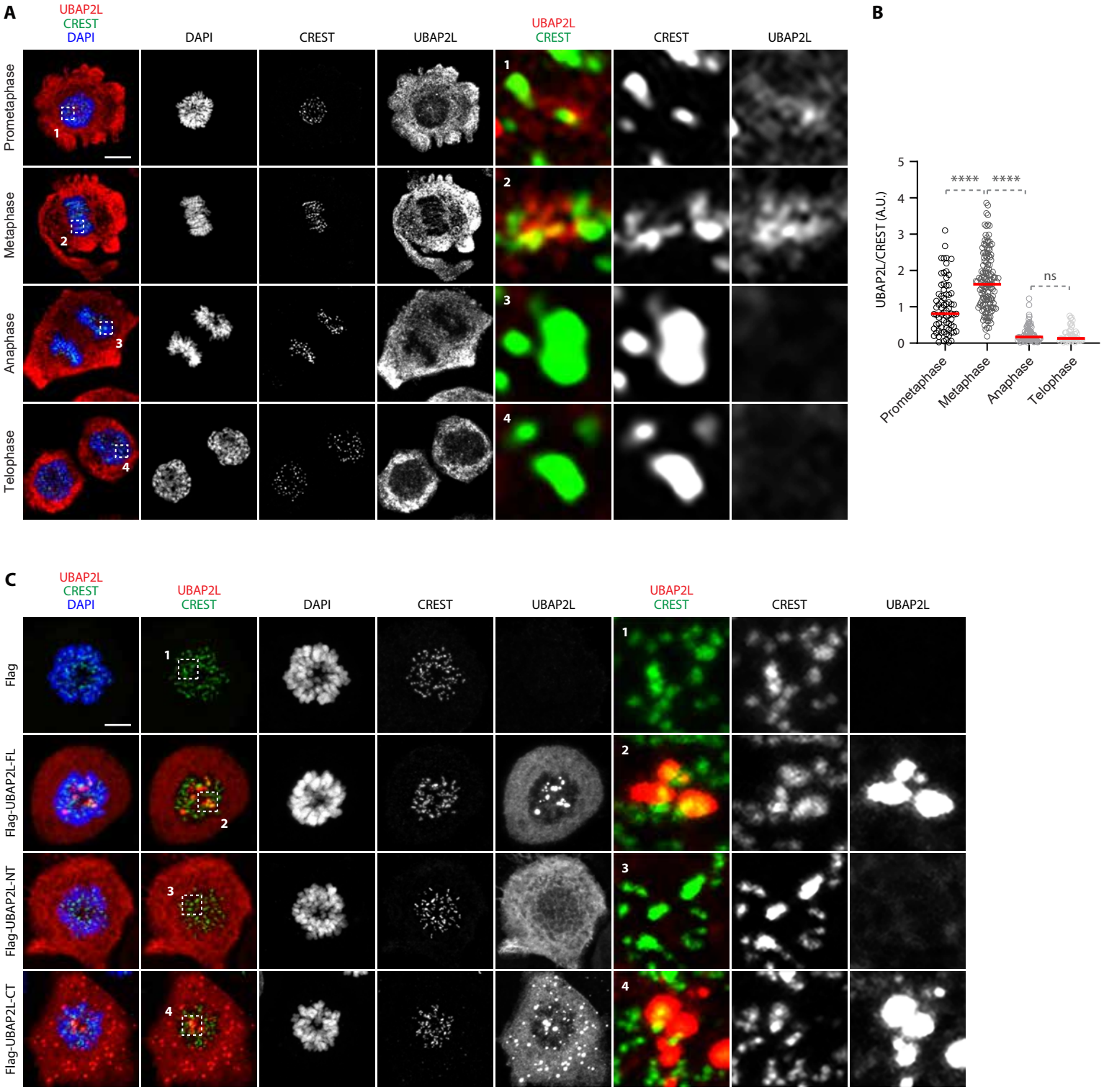

Figure 8.

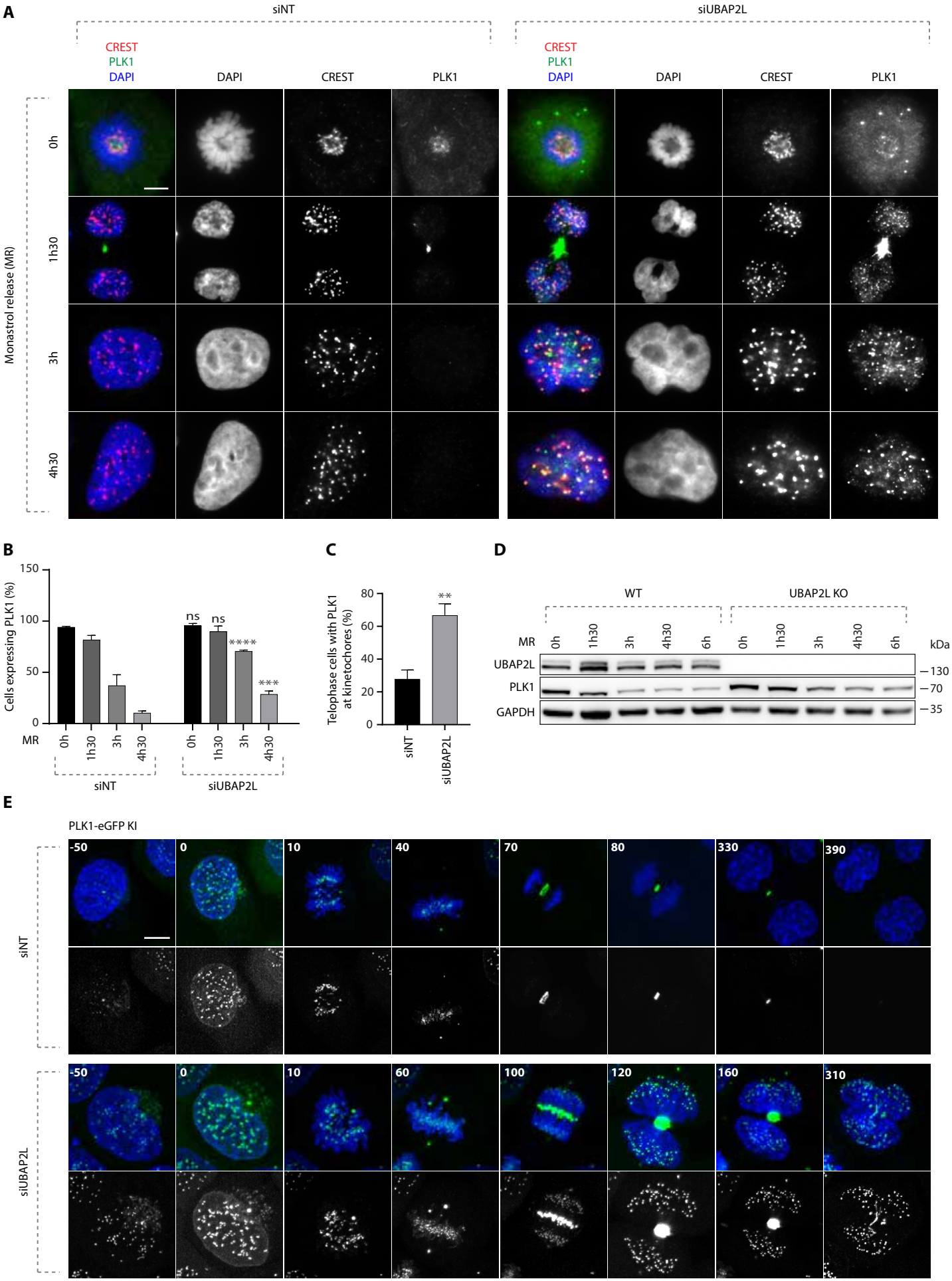

Figure 9.